

## NGC 2770 - A SUPERNOVA IB FACTORY? \*

CHRISTINA C. THÖNE<sup>1</sup>, MICHAŁ J. MICHAŁOWSKI<sup>1</sup>, GIORGOS LELOUDAS<sup>1</sup>, NICK L. J. COX<sup>2</sup>, JOHAN P. U. FYNBO<sup>1</sup>,  
JESPER SOLLERMAN<sup>1,3</sup>, JENS HJORTH<sup>1</sup> AND PAUL M. VREESWIJK<sup>1</sup>*Draft July 2008*

## ABSTRACT

NGC 2770 has been the host of three supernovae of Type Ib during the last 10 years, SN 1999eh, SN 2007uy and SN 2008D. SN 2008D attracted special attention due to the serendipitous discovery of an associated X-ray transient. In this paper, we study the properties of NGC 2770 and specifically the three SN sites to investigate whether this galaxy is in any way peculiar to cause a high frequency of SNe Ib. We model the global SED of the galaxy from broadband data and derive a star-formation and SN rate comparable to the values of the Milky Way. We further study the galaxy using longslit spectroscopy covering the major axis and the three SN sites. From the spectroscopic study we find subsolar metallicities for the SN sites, a high extinction and a moderate star-formation rate. In a high resolution spectrum, we also detect diffuse interstellar bands in the line-of-sight towards SN 2008. A comparison of NGC 2770 to the global properties of a galaxy sample with high SN occurrence ( $\geq 3$  SN in the last 100 years) suggests that NGC 2770 is not particularly destined to produce such an enhancement of observed SNe observed. Its properties are also very different from gamma-ray burst host galaxies. Statistical considerations on SN Ib detection rates give a probability of  $\sim 1.5\%$  to find a galaxy with three Ib SNe detected in 10 years. The high number of rare Ib SNe in this galaxy is therefore likely to be a coincidence rather than special properties of the galaxy itself. NGC 2770 has a small irregular companion, NGC 2770B, which is highly starforming, has a very low mass and one of the lowest metallicities detected in the nearby universe as derived from longslit spectroscopy. In the most metal poor part, we even detect Wolf-Rayet features, against the current models of WR stars which require high metallicities.

*Subject headings:* galaxies: ISM, galaxies: NGC 2770

## 1. INTRODUCTION

Massive stars end their lives in various ways, as governed by their mass, composition, angular momentum and whether or not they are interacting with a companion star (e.g. Heger et al. 2002). The most massive stars lose their outer layers through winds whose strength strongly depend on the metallicity of the star (e.g. Crowther et al. 2002, and references therein). These stripped stars explode as supernovae (SNe) Type Ib (SN Ib) if they have lost their hydrogen envelope or as SNe Type Ic (SN Ic) if they have also lost their He envelope. If the star is also rapidly rotating, it is believed that the star might even produce a Gamma-Ray Burst (GRB) (MacFadyen & Woosley 1999; Woosley & Heger 2006). SNe Ib/c are much rarer than SNe II, which are produced by stars with masses of 8 to 40  $M_{\odot}$ , whereas SNe Ib/c are assumed to require zero age main sequence (ZAMS) masses of  $\gtrsim 35 M_{\odot}$  for non-rotating stars (Woosley et al. 2002). GRBs are even less common than SNe Ic which is in line with the general picture that GRB progenitors require some special conditions to produce a GRB.

Only for SNe II has it been possible to identify the progenitor star - which turned out to be yellow, red or

blue giants with masses of around 8 – 20  $M_{\odot}$ , e.g. SN 1987A (Gilmozzi et al. 1987), SN 2002ov (Li et al. 2007), SN 2004A (Hendry et al. 2006) and SN 2006gl (Gal-Yam et al. 2007). Furthermore, several detections have been made using preexplosion imaging from the *HST* archive (e.g. Smartt et al. 2003). SNe Ib/c have so far evaded an identification with a progenitor star (Maund et al. 2005; Crockett et al. 2007, 2008). This is also the case for GRBs which most often occur at distances that do not even allow us to resolve their host galaxies.

When the progenitor cannot be directly identified, studying the environment can provide important information about what kind of star exploded. Spatially resolved photometric studies of the sites of different types of SNe show that SNe Type II trace the light of their host galaxies while GRBs are more concentrated towards bright regions (Fruchter et al. 2006) and that SNe Type Ib, Ic and GRBs appear to be differently distributed within their hosts (Kelly et al. 2007). Spectroscopic investigations show that the broadlined SNe Ic which are not connected to GRBs are found at sites with higher metallicities than those that are connected to GRBs (Modjaz et al. 2008a). A spatially resolved study of the host of one long-duration GRB which was not connected to a SN also showed a low metallicity in comparison to the rest of the host galaxy (Thöne et al. 2008).

Long duration GRBs have been found to be associated with broadlined SNe Ic. There are four spectroscopically confirmed cases so far, namely GRB 980425 (Galama et al. 1998), GRB 030329 (Hjorth et al. 2003; Matheson et al. 2003; Stanek et al. 2003), GRB 031203 (Cobb et al. 2004; Thomsen et al. 2004; Malesani et al. 2004; Gal-Yam

\*BASED ON OBSERVATIONS WITH THE NORDIC OPTICAL TELESCOPE, ESO PROPOSAL 080.D-0526, THE GALEX AND NED DATABASES

<sup>1</sup> Dark Cosmology Centre, Niels-Bohr-Institute, University of Copenhagen, Juliane Maries Vej 30, 2100 København Ø, Denmark<sup>2</sup> Herschel Science Centre, European Space Astronomy Centre, ESA, P.O.Box 78, E-28691 Villanueva de la Cañada, Madrid, Spain<sup>3</sup> Stockholm Observatory, Alba Nova, 10691 Stockholm, Sweden  
Electronic address: cthoene@dark-cosmology.dk

et al. 2004) and GRB 060218 (Pian et al. 2006; Sollerman et al. 2006; Modjaz et al. 2006; Mirabal et al. 2006). For all other nearby long GRBs up to 2006 where a SN could have been observed, additional light from the SN component was found in the late time lightcurves (e.g., Zeh et al. 2004). GRBs therefore offer a unique opportunity to observe a SN from the very onset of the explosion, as indicated by the prompt emission from the GRB. The connection between GRBs and broadlined SNe Ic, however, had to be revised in 2006 when two long-duration GRBs were found not to show any sign of an associated SN (Fynbo et al. 2006; Gehrels et al. 2006; Della Valle et al. 2006; Gal-Yam et al. 2006; Ofek et al. 2007).

One important supernova that recently caught the attention of the community is SN 2008D which was associated with an X-ray transient (XT) (Soderberg et al. 2008). This supernova was serendipitously detected while the XRT instrument onboard the *Swift* satellite (Gehrels et al. 2004) observed another supernova, SN 2007uy, in the same galaxy. Whether this prompt XT originated from a weak GRB-like event or if it was due to the shock breakout from the star is still under debate (Soderberg et al. 2008; Modjaz et al. 2008b; Malesani et al. 2008; Xu et al. 2008). The X-ray emission, however, is clearly associated with the onset of the explosion, and consequently SN 2008D was one of the earliest observed SNe. The SN spectrum evolved from a smooth spectrum with small undulations characteristic of a high-velocity ejecta into a typical SN Ib (Soderberg et al. 2008; Modjaz et al. 2008b; Malesani et al. 2008). Also the host galaxy of this supernova, NGC 2770, has attracted some attention as it produced three SNe within the last 9 years, SNe 1999eh, 2007uy and 2008D. Intriguingly, all three were stripped envelope core-collapse SNe Ib.

In this paper, we present a study on the local properties at the SN sites as well as of other regions in NGC 2770 with longslit spectroscopy and compare the host itself with a sample of other supernova producing galaxies. We want to investigate if the occurrence of three recent SNe Ib can be explained by some physical properties of the host galaxy. In Section 2 we present the observations and data reduction of the spectra, Section 3 studies the global properties of NGC 2770 and properties derived from modeling the spectral energy distribution (SED). In Section 4 we analyze the different regions in the host in terms of metallicity, extinction and star formation rate (SFR). Section 5 compares NGC 2770 to a sample of other nearby galaxies with several recent SNe and discuss the probability to find three SNe Ib in a galaxy within nine years. Finally, Section 6 investigates the properties of the companion galaxy NGC 2770B. Throughout the paper we use a cosmology with  $H_0=70 \text{ km s}^{-1} \text{ Mpc}^{-1}$ ,  $\Omega_\Lambda=0.7$  and  $\Omega_m=0.3$ . At  $z=0.007$  this corresponds to 0.13 kpc per arcsecond and we use a distance of 27 Mpc to NGC 2700.

## 2. OBSERVATIONS

We carried out optical spectroscopy using the FORS2 spectrograph at the VLT on Jan. 11.31, 2008. A  $1''.0$  arcsec wide slit together with the 300V grism provided a resolution of 11 Å. The slit covered the site of SN 2008D as well as some outer parts of the galaxy. We obtained further spectra with ALFOSC at the NOT on Jan. 13, 15 and on Feb. 03 using grism 4. These observations were

TABLE 1  
OBSERVATION LOG

Date [UT]	telescope/instr.	grism/filter	$\lambda, \lambda_c/\Delta\lambda$ [Å]	exptime [s]
Jan. 11.31	VLT/FORS2	grism 300V	3000–9600	600
Jan. 13.07	NOT/ALFOSC	grism 4	2950–9050	3600
Jan. 15.21	NOT/ALFOSC	grism 4	2950–9050	600
Jan. 15.95	NOT/ALFOSC	grism 4	2950–9050	3600
Jan. 18.22	VLT/UVES	DIC1	3300–6650	3600
Feb. 03.15	NOT/ALFOSC	grism 4	2950–9050	1800
Mar. 16.11	VLT/FORS1	H $\alpha$ $z=0.007$	6604 / 64	120
Mar. 16.11	VLT/FORS1	H $\alpha$ $z=0$	6563 / 61	120

NOTE. — Log of the spectroscopic and narrowband imaging observations.

also part of the observations reported in Malesani et al. (2008). While Malesani et al. (2008) used these data to study the supernova itself, we instead concentrate on the host galaxy. The three NOT spectra were obtained at three different slit positions (see also Fig. 4). The first included the positions of SNe 2008D and 2007uy which were also detected in the spectrum. The second one was placed along the major axis of the galaxy and the last one included the positions of SNe 2008D and 1999eh, where the latter one had already faded. On Jan. 15.21, we also obtained one 600s spectrum of the nearby galaxy NGC 2770B with ALFOSC (Fynbo et al. 2008). Reduction and flux calibration of the spectra were done using standard tasks in IRAF. For the flux calibration we used the standard stars HD 19445, BD+75325 and BD+332642 for the ALFOSC spectra and GD 108 for the FORS2 spectrum. From the longslit spectra we then extracted traces of equal sizes at the positions of the SNe and other HII regions in the galaxy (see Section 4)

Furthermore, we obtained high-resolution echelle spectra of SN 2008D with UVES (Dekker et al. 2000) at the VLT on Jan. 18, 2008. We used the DIC1 (390+564) setting together with a  $1''.0$  wide slit. This set-up covers a wavelength range from 3300 to 6650 Å at a resolution of 6–8 km s $^{-1}$ . The UVES data have been reduced and extracted using the ESO CPL pipeline<sup>4</sup> and flux-calibrated with the master response curves provided by ESO<sup>5</sup>.

We also obtained imaging data with FORS1 at the VLT on March 16 using an H $\alpha$  filter shifted to  $z=0.007$  with a central wavelength of 6604 Å and a width of 64 Å as well as an offband filter for which we used the H $\alpha$  filter at  $z=0$  with  $\lambda_{\text{center}} = 6563 \text{ Å}$  and  $\Delta\lambda = 61 \text{ Å}$ . In order to flux calibrate the H $\alpha$  image we determined the flux within the H $\alpha$  line from one of the traces extracted from the FORS spectra. We compared this flux with the counts within several rectangular apertures of the same size as for the extraction of the spectrum ( $1 \times 3 \text{ arcsec}$ ) at the same positions along the slit by accounting for the different continuum levels from the galaxy and the varying strength of the [N II] line which is included in the H $\alpha$  narrowband filter.

For a log of the observations see Table 1. Fig. 1 shows a color composite of I band observations taken with FORS1 (Malesani et al. 2008) and the H $\alpha$  and H $\alpha$  offband images used in this paper.

<sup>4</sup> <http://www.eso.org/sci/data-processing/software/pipelines/uves/uves-pipe-recipes.html>

<sup>5</sup> <http://www.eso.org/observing/dfo/quality/UVES/qc-response.html>

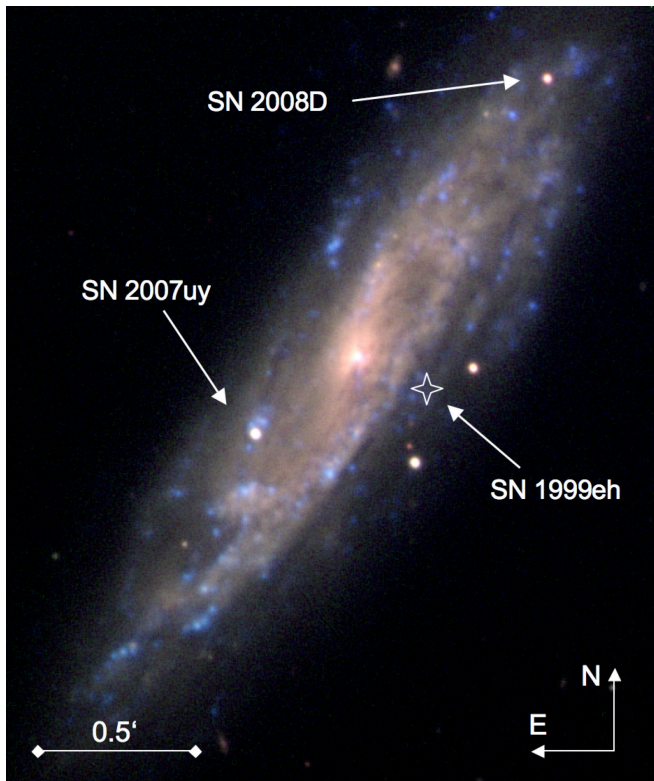


FIG. 1.— Image of NGC 2770 from I (red color), H $\alpha$  (blue) and H $\alpha$  offband (green) filters. The field of view is about  $2 \times 2.5$  arcmin. Blue indicates H $\alpha$  emission which nicely show the SF regions in the spiral arms of the galaxy. The positions of the 3 SNe are shown of which two are still visible in the image.

### 3. GLOBAL PROPERTIES OF NGC 2770

#### 3.1. Modelling of the spectral energy distribution

Extensive data are available in the literature on the emission of NGC 2770 at various wavelengths. We performed photometry on the archival *GALEX* (Martin et al. 2003, 2005) UV images and Sloan Digital Sky Survey (SDSS) *ugriz* images. Furthermore, we obtained the infrared and radio fluxes from Cutri et al. (2003); Moshir et al. (1990); Dressel & Condon (1978) and Condon et al. (1998) reported in the NASA Extragalactic Database (NED). These data were used to fit the broad band spectral energy distribution (SED) with templates from the GRASIL code (Silva et al. 1998).

In the GRASIL code each SED template is calculated by the following procedure. At the first stage an initial gas reservoir, infalling gas rate and star formation history are assumed and then at given time the emission of the resulting stellar population is summed up. Finally, the total galaxy spectrum is calculated by means of a two-dimensional radiative transfer method, applied to photons reprocessed by dust. After we found the best-fitting template we derived several galaxy properties from the SED (as in Michałowski et al. 2008). SFR, SN rate, stellar, dust, gas and total baryonic masses are given as output from GRASIL for the best-fitting template. The Infrared luminosity was obtained by integrating the SED over the range of  $8 - 1000 \mu\text{m}$ . The average extinction (outside of the molecular clouds) was calculated as:  $A_V = 2.5 \log (V\text{-band starlight extinguished by molecular clouds only} / V\text{-band starlight observed, see Silva et al. (1998))$ . This parameter describes the ex-

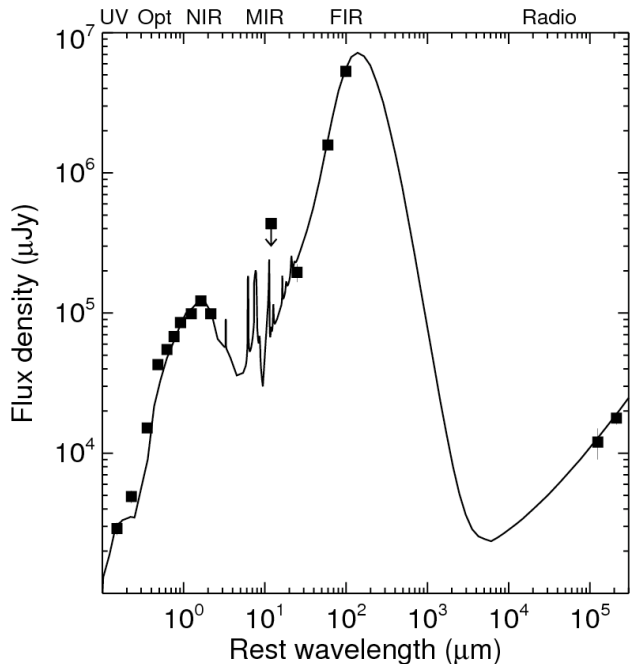


FIG. 2.— Modelling of the broad-band SED of NGC 2770 from UV to radio wavelength using archival data compiled from the NASA Extragalactic Database (NED) and publicly available optical and ultraviolet data from the SDSS and GALEX archives. Error bars are mostly smaller than the symbols. The solid line shows the best-fit model from the GRASIL code (Silva et al. 1998), which is the average of Sb and Sc templates (based on NGC 6946).

inction averaged throughout the galaxy as opposed to the line-of-sight extinction derived from optical GRB afterglows.  $R_V$  was calculated comparing the extinction in the V- and B-bands:  $R_V = A_V / E(B - V)$ .

The spectral energy distribution (SED) of NGC 2770 is well represented by an average model composed of the spiral Sc (NGC 6946) and Sb galaxies, taken from Silva et al. (1998). From the SED fit (see Fig. 2) we derive a star-formation rate (SFR) of  $\sim 1.1 M_\odot \text{ yr}^{-1}$  and a stellar mass of  $2.1 \times 10^{10} M_\odot$  (see Michałowski et al. 2008, for details on how these are derived from the SEDs). The resulting specific star-formation rate (SSFR) is  $0.05 \text{ Gyr}^{-1}$ . The SFRs derived from different methods (radio, IR, UV, SED modelling) differ by about a factor of 2. This is not surprising since the UV SFR estimate is affected by extinction and the different methods trace different parts of SF in the galaxy. Still, the values indicate that the SFR is not particularly high in NGC 2770. The SFR in radio is also directly connected to the supernova rate (SNR) as the nonthermal radio flux is produced by relativistic electrons accelerated in the SN shocks. Also the supernova rate (SNR) both from radio data and the SED modelling is therefore rather low with  $0.01\text{--}0.02 \text{ SNe yr}^{-1}$  which is comparable to the SNR of the Milky Way (MW). In addition to the SED fit, we also searched the literature for global measurements and properties of NGC 2770. Those, together with the SED outputs, are presented in Table 2.

#### 3.2. NGC 2770 in the context of other spiral galaxies

In order to quantify to what extent the properties of NGC 2770 are similar to other galaxies we compare the global properties of NGC 2770 with a sample of more than 100 nearby spiral galaxies from Broeils & Rhee

(1997) which also includes NGC 2770. This sample is based on two HI surveys of spiral and irregular galaxies with the Westerbork Synthesis Radio Telescope. We then determine the median and mean values of a number of properties and compare that with the values derived for NGC 2770. The mean in this sample is dominated by a few extreme outliers in the sample, therefore, we prefer to take the median value for comparison. We then conclude the following:

- The HI surface density is one of the highest in the sample (median:  $3.65 \text{ M}_\odot/\text{pc}^2$ , maximum:  $8.05 \text{ M}_\odot/\text{pc}^2$ , NGC 2770:  $4.99 \text{ M}_\odot/\text{pc}^2$ ).
- The HI mass is also above average (median:  $3.5 \times 10^9 \text{ M}_\odot$ , NGC 2770:  $7 \times 10^9 \text{ M}_\odot$ ).
- The total mass is above the median but slightly below the mean, however this is dominated by some very massive galaxies (median:  $\log M_{\text{tot}} = 7.8 \text{ M}_\odot$ , NGC 2770:  $\log M_{\text{tot}} = 11.38 \text{ M}_\odot$ ).
- The ratio of the gas mass to the blue (*B*-band) luminosity is close to average (median:  $0.26 \text{ M}_\odot/L_{B\odot}$ , NGC 2770:  $0.24 \text{ M}_\odot/L_{B\odot}$ ).
- The ratio of the gas mass to the near-IR (*H*-band) luminosity is slightly above average (median:  $0.31 \text{ M}_\odot/L_{H\odot}$ , NGC 2770:  $0.44 \text{ M}_\odot/L_{H\odot}$ ).
- The ratio of the gas mass to the total mass is slightly above average (median:  $0.05$ , NGC 2770:  $0.06$ ).

This comparison shows that NGC 2770 has more or less average properties within this sample, except for the HI mass. The rather high gas mass and HI surface density indicate that there is a lot of material present to produce stars. However, the current and past SFRs as derived from different datasets (see also Section 4.3) are not at all exceptionally high. Soderberg et al. (2008) suggested that the companion galaxy NGC 2770B could be interacting with NGC 2770 and cause the enhancement in SF. No obvious perturbations are visible in the optical images of NGC 2770. It would be interesting to investigate possible perturbations in the HI velocity field, but the available data from VLA do not provide a good enough resolution. Wainwright et al. (2007) conclude from *HST* imaging of GRB host galaxies that about 30–50% show evidence for interaction. However, the host of GRB 980425/SN 1998bw was found to be an isolated galaxy (Foley et al. 2006) and the SF history is also consistent with a constant SFR over a few Gyrs (Sollerman et al. 2005).

#### 4. SPATIALLY RESOLVED OPTICAL SPECTROSCOPY OF NGC 2770

From the four 2-dimensional longslit spectra, we extracted traces at all positions along the slit that showed emission in  $\text{H}\alpha$ . We chose equally large extraction windows in all the spectra with a width of 3 arcsec, corresponding to 0.43 kpc. The spectra were then extracted using the strong and well defined SN traces as templates. For the slit containing SNe 2008D and 2007uy we took the SN trace closest to the region we wanted to extract. The relative distortions along the spatial axis are however

only within one to two pixels and even for spectra with only one template trace, we are confident that we extracted the same region along the entire dispersion axis. We note here that the FORS spectrograph has an atmospheric dispersion corrector while ALFOSC has none. This implies that the ALFOSC slit do not necessarily trace the same physical region in the blue and in the red part of the spectra. However, the airmass at the time of the observations was very low and the expected refraction should be negligible.

For the wavelength calibration, we extracted several traces from the arc spectrum with the SN trace as a template and shifted to different positions along the spatial axis. In each of these traces we identified the arc lines and wavelength calibrated the different parts along the slit with the nearest arc spectrum trace. Fortunately, the distortion of the arclines along the entire chip is also within a few pixels. The maximum deviation between the arclines at the extracted trace and the position taken for the arcspectrum should be less than 1 pixel which corresponds to an accuracy of  $0.3 \text{ \AA}$  comparable to the accuracy from the wavelength calibration itself. Finally, we flux calibrated the individual spectra using the corresponding standard stars observed at the same night and the same setting. We note that the flux of an extraction window is different from the one of a pointsource as the point spread functions from the neighbouring pixels in the spatial direction extend into the extracted part.

We then fitted the emission lines present in the spectra with Gaussians and measured the fluxes and, where possible, the equivalent widths (EW) of the  $\text{H}\alpha$  line. For the SN regions, the latter is prevented by the contamination from the SN continuum. In a few cases, deblending the [N II] and  $\text{H}\alpha$  lines in the ALFOSC spectra proved to be difficult at this low resolution. In some regions, it seems that the part covered by the slit actually contains two kinematically different regions as the  $\text{H}\alpha$  lines shows a double peak which then blends with the bluer component of the corresponding [N II] double peak. This is not surprising since we observe NGC 2770 at a small inclination. Regions with heavily blended lines were discarded from the analysis. The properties in the different regions derived from the emission line analysis as present in the next sections are listed in Tab. 3 and plotted in Fig. 3.

##### 4.1. Metallicity

For the different regions along the slits we estimated the metallicity using the N2 parameter. This is the ratio between [N II]/ $\text{H}\alpha$  and is calibrated as  $12 + \log(\text{O}/\text{H}) = 9.37 + 2.03 \times \text{N2} + 1.26 \times \text{N2}^2 + 0.32 \times \text{N2}^3$  (Pettini & Pagel 2004). In the regions with significant detection of [O III], we also use the O3N2 parameter,  $\text{O3N2} = \log[(\text{O III } \lambda 5007 / \text{H}\beta) / (\text{N II} / \text{H}\alpha)]$ , to derive metallicities with  $12 + \log(\text{O}/\text{H}) = 8.73 - 0.32 \text{ O3N2}$  (Pettini & Pagel 2004).

The O3N2 parameter has been calibrated against oxygen abundances derived directly by determining the electron temperature  $T_e$  from the temperature sensitive [O III]  $\lambda 4363$  line (e.g. Izotov et al. 2006). The O3N2 parameter is also considered as the most reliable method by Kewley & Dopita (2002), if the spectra could be corrected for dust extinction. However, for low metallicities, the [O III]  $\lambda 5007$  line becomes very weak. We were not able to use it for deriving metallicities everywhere, since

TABLE 2  
GLOBAL PROPERTIES OF NGC 2770

Property	Value	Notes	Reference
SFR (SED)	$1.1 \text{ M}_\odot \text{ yr}^{-1}$		this work
SFR (radio)	$0.6 \text{ M}_\odot \text{ yr}^{-1}$	using Yun & Carilli (2002)	this work
LIR	$1.4 \times 10^{10} \text{ L}_\odot$		this work
SFR (IR)	$1.22 \text{ M}_\odot \text{ yr}^{-1}$	using Kennicutt (1992, eq. 4)	this work
SFR (UV)	$0.50 \text{ M}_\odot \text{ yr}^{-1}$	using Kennicutt (1992, eq. 1)	this work
$v_{\text{rot}}^{\text{max}}$	$152 \text{ km s}^{-1}$	21cm emission	(Rhee & Albada 1996)
$M_{\text{gas}}$	$1.9 \times 10^9 \text{ M}_\odot$		this work
$N_{\text{HI}}$	$1.6 \times 10^{20} \text{ atom cm}^{-2}$		(Staveley-Smith & Davies 1988)
$M_{\text{HI}}$	$7 \times 10^9 \text{ M}_\odot$		(Broeils & Rhee 1997)
$M_{\text{star}}$	$2.1 \times 10^{10} \text{ M}_\odot$	SED	this work
$M_{\text{tot}}$	$2.6 \times 10^{10} \text{ M}_\odot$	SED	this work
$M_{\text{tot}}$	$1.1 \times 10^{11} \text{ M}_\odot$	including DM; from $v_{\text{rot}}$	(Broeils & Rhee 1997)
$M_{\text{dust}}$	$1.9 \times 10^7 \text{ M}_\odot$	SED	this work
$M_{\text{BH}}$	$1.3 \times 10^6 \text{ M}_\odot$		(Dong & Robertis 2006)
SN rate SED	$0.02 \text{ SN yr}^{-1}$		this work
SN rate radio	$0.01 \text{ SN yr}^{-1}$	using Condon (eq. 18 in 1992)	this work
$A_V$	0.15 mag	SED	this work
$A_B$	0.19 mag	SED	this work
$A_B$	0.14 mag	from $N_{\text{HI}}$	(Staveley-Smith & Davies 1988)
$E(B-V)$	0.03 mag	SED	this work
$E(B-V)$	0.84 mag	Balmer decrement, global	(Ho et al. 1997)
$R_V$	4.3	SED	this work
$n_e$	$54 \text{ cm}^{-3}$	(electron density)	(Ho et al. 1997)

in some parts of the spectra it was only detected with very low significance. For consistency, we therefore use the N2 estimate throughout this article. The N2 parameter does, however, saturate at about solar metallicity and even turns around at higher metallicities (about twice solar). This is not a problem in our data as we do not have regions where the O3N2 parameter gives supersolar metallicities while the N2 metallicity gives a subsolar value.

We find that the N2 and the O3N2 methods give rather consistent results at the sites where both are determined. The error of the O3N2 parameter is about 0.2 dex in the ALFOSC spectra and 0.10–0.15 in the FORS slit. The metallicities from the O3N2 and N2 parameters have systematic errors of 0.14 dex for O3N2 and 0.18 for N2. We therefore estimate the total error of each metallicity value to be 0.2 dex for both O3N2 and N2. In Fig. 3 we plot the results from both methods where available. Figure 4 visualizes the 2D distribution of the N2 metallicities in the different parts of the galaxy as probed by the four slits.

The metallicity at the SN sites derived from N2 are  $12+\log(\text{O}/\text{H}) \sim 8.4, 8.5$  and  $8.4$  for SNe 2008D, 2007uy and 1999eh respectively, which corresponds to  $0.55\text{--}0.70 Z_\odot$  [when using 8.66 for the Sun Asplund et al. (2004)]. The metallicities derived at the position of SN 2008D differ between the ALFOSC and the FORS slits, but still agree within the errors. We therefore adopt an average metallicity of  $8.4$  for SN 2008D. The other regions in the outer spiral arms on both sides of the galaxy give similar values for the metallicity for different slits. The nucleus and the central regions have solar or supersolar metallicity. From this we derive a metallicity gradient of  $-0.06$  dex per kpc. The average metallicity computed from the values along the major axis of the galaxy is  $8.4$ .

It is interesting to note that the metallicities at the SN Ib sites in NGC 2770 lie between the low values found for GRB connected broadline SNe Ic and those of broadline

SNe Ic not connected to GRBs (Modjaz et al. 2008a). They are also slightly higher than the metallicity of the HII region which hosted SN 1998bw, a broadlined SN Ic connected to GRB 980425, as determined from IFU observations of the host (Christensen et al. 2008). Also the site of the SN-less GRB 060505 (Thöne et al. 2008) had a lower metallicity as the SN Ib sites in NGC 2770. It seems, GRB related SNe have a rather low metallicity while SNe Ib have about half solar to solar metallicities whereas (broadline) SNe Ic require solar to slightly above solar metallicities. This result seems consistent with the suggestion that in nonrotating stars, the mass loss scales with the metallicity (e.g Crowther et al. 2002) and SN Ic progenitors are likely experiencing larger mass loss than SNe Ib. Fast rotating stars, however, as required by the collapsar model (MacFadyen & Woosley 1999), should preferentially have low metallicities and less mass loss in order to keep the high angular momentum, which is required to produce a GRB.

#### 4.2. Extinction

The extinction throughout the galaxy is estimated from the Balmer decrement. Since  $H\gamma$  is not detected, we can only use the  $H\alpha/H\beta$  ratio (Osterbrock 1989). The derived extinction is generally high with values for  $E(B-V)$  between 0.4 and 3.7 mag with most of the regions having  $E(B-V) \sim 1$  mag. The extinction at the SN sites is considerable with  $E(B-V)=0.9$  mag for SN 2008D, 1.4 mag for SN 2007uy and 0.7 mag for SN 1999eh. Malesani et al. (2008) get a value of  $E(B-V)=0.8$  mag from fitting the SN SED, while (Modjaz et al. 2008b) adopt  $0.6 \pm 0.1$  from the SN broadband fit. The Galactic extinction towards NGC 2770 is negligible with  $E(B-V)=0.02$  mag (Schlegel et al. 1998).

Further evidence for dust extinction along the line of sight towards SN 2008D comes from the detection of NaD absorption in the UVES high resolution spectra, the EWs measured are listed in Tab. 4. For unsaturated

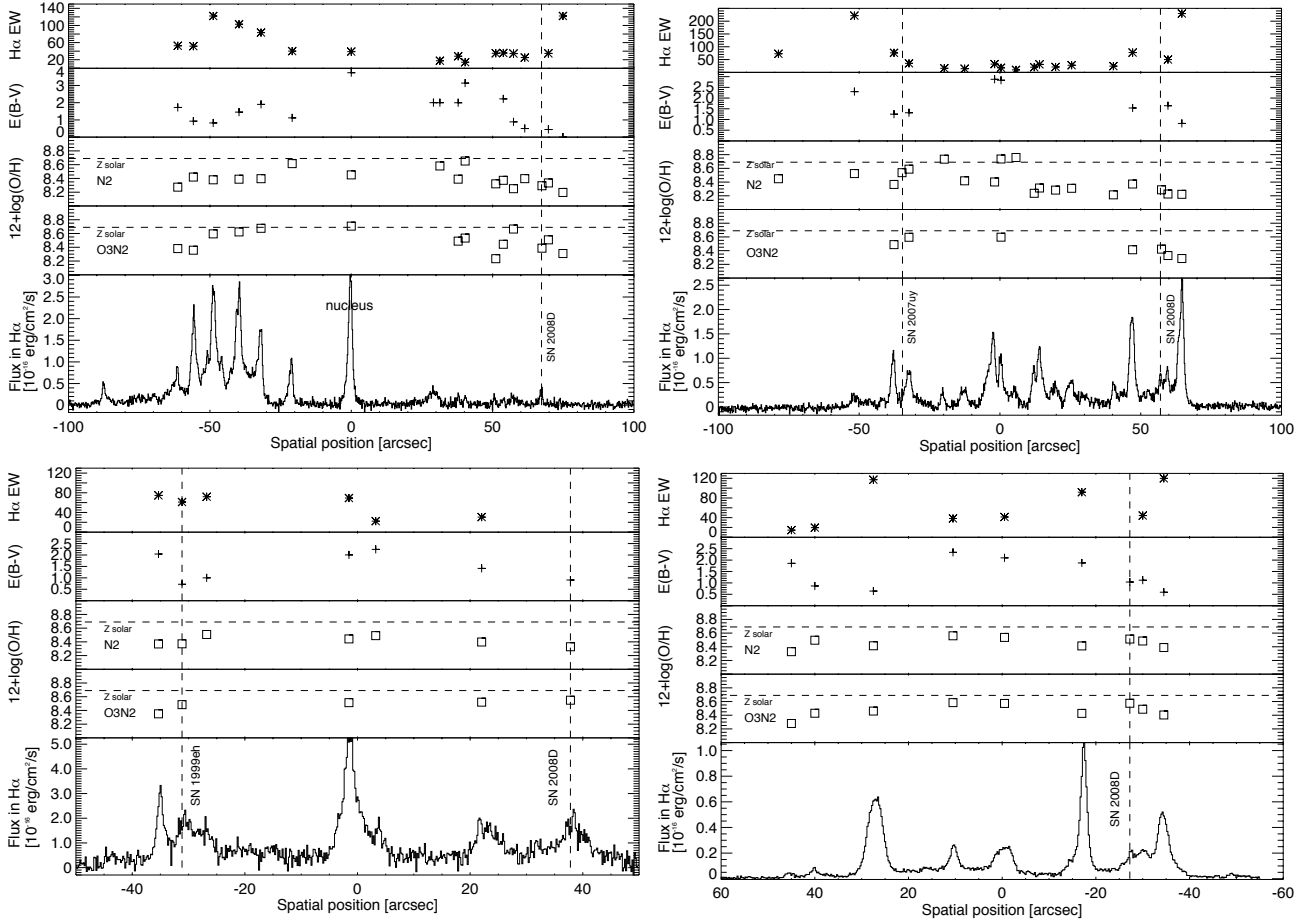


FIG. 3.— Cut through the H $\alpha$  line and the properties at the different HII regions (see Fig. 4 for the slitpositions on the galaxy). We plot two calibrations for the metallicity (errors are 0.2 dex for both methods), the extinction E(B-V) in [mag] and the H $\alpha$  EW in [ $\text{\AA}$ ]. The four panels are: upper left: ALFOSC slitposition covering the major axis of the galaxy (slit1), upper right: the slit going through the sites of SN 2008D and SN 2007uy (slit2), lower left: position including SN 2008D and 1999eh (slit3) and lower right: the FORS slitposition (slit4). For the slit along the major axis, spatial position = 0 kpc indicates the center of the galaxy, for the other positions, for the other slits, 0 arcsec was chosen randomly.

and mildly saturated lines, there is a direct relation between the strength of the Na D absorption and the extinction (Munari & Zwitter 1997) which have been calibrated towards stars in the LMC. Taking the EW for the two components together, we get an extinction of  $E(B-V)=1.1$  mag. However, Munari & Zwitter (1997) note that systems with such high EWs are usually consisting of several components and the extinction of different components is additive so it is more appropriate to add the extinction of the resolved subcomponents which are on the linear part of the EW-E(B-V) relation. The two components then give  $E(B-V)_1 = 0.14$  and  $E(B-V)_2 = 0.18$  mag and therefore  $E(B-V)_{\text{tot}} = 0.32$  mag. There is also a high  $N_H$  column derived from the X-ray spectra (Soderberg et al. 2008) of  $N_H = (7 \pm 1) \times 10^{21} \text{ cm}^{-2}$ , assuming Galactic abundances. The corresponding gas-to-dust ratio of  $2.8 \times 10^{21} \text{ cm}^{-2} \text{ mag}^{-1}$  is low (close to the Galactic ratio  $N_H = 1.7 \times 10^{21} \text{ cm}^{-2} \text{ mag}^{-1}$ ) compared to the ratios observed in GRB host galaxies that are typically an order of magnitude higher, suggesting that NGC 2770 is dust-rich compared to those hosts.

We also detect a number of diffuse interstellar bands (DIBs) at  $\lambda\lambda$  5821.5  $\text{\AA}$ , 5837.4  $\text{\AA}$  and 6328.0  $\text{\AA}$  in the UVES spectra which indicates the presence of dust at the site of SN 2008D. DIBs are speculated to be pro-

duced by large carbon molecules, possibly related to the polycyclic aromatic hydrocarbons (PAHs) that produce strong fluorescence lines in the mid-infrared. It is interesting to note that DIBs have never been detected in the afterglow spectra of GRBs suggesting a harder radiation field and younger stars in those galaxies compared to NGC 2770. We fit the observed spectra (rebinned to 0.09  $\text{\AA}$ ) with template DIB profiles obtained from high-resolution high-S/N spectra of DIBs in the diffuse cloud toward HD 144217. We keep the width of the feature fixed but leave the continuum, the central wavelength and the depth scaling as free parameters. Doppler broadening due to the different velocity components as fitted from the NaD and Ca II absorption in the UVES spectra (see Section 4.4) is negligible for the broad  $\lambda$  6283 and  $\lambda$  5780 DIBs (FWHM  $\sim 100$  and  $\sim 200 \text{ km s}^{-1}$ ). For the narrow  $\lambda$  5797 DIB (FWHM  $\sim 40 \text{ km s}^{-1}$ ) we assume that DIBs are present in similar abundance in both cloud components as is the case for the Ca II absorption strengths. Taking into account the two components increases the derived  $\lambda$  5797 DIB strength by about 10-15%.

Diffuse interstellar bands can provide an important measure, just as Na I and K I, for the amount of dust in line-of-sights probing the diffuse interstellar medium.



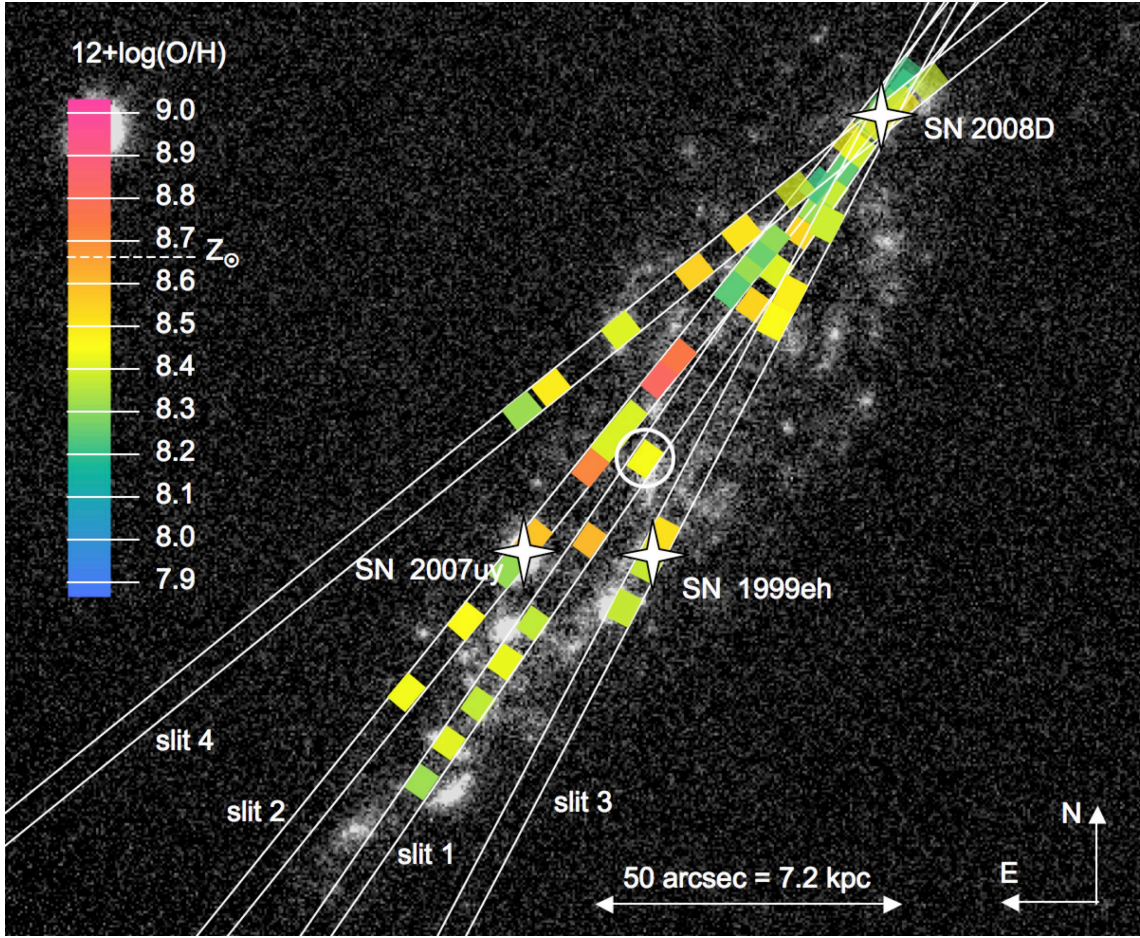


FIG. 4.— Metallicities in NGC 2770 along the 4 slitpositions as described in Fig. 3 including the 3 SN sites derived from the  $[\text{N II}]/\text{H}\alpha$  ratio. The image of the galaxy was taken with the  $\text{H}\alpha$  filter in order to highlight the starforming regions. The circle indicates the center of the galaxy.

Additionally, the behavior of different DIBs (or DIB ratios) in the Milky Way can be used to gain insight in the local physical conditions of extra-galactic diffuse clouds. The  $\lambda 5780$  DIB carrier is sensitive to UV radiation and becomes stronger when exposed to sufficient UV (at which time for example the  $\lambda 5797$  DIB carrier is already being destroyed by this radiation). For example, the DIB strengths (strong  $\lambda 5780$  and  $\lambda 6283$  DIBs) toward SN2001el in NGC 1448 suggest a strong local UV field (Sollerman et al. 2005). On the other hand, observations of the ISM toward SN2006X in M100 (Cox & Patat 2008) indicate a dense environment protected from strong UV radiation as it shows a very weak  $\lambda 6283$  DIB and the presence of di-atomic molecules. The  $\lambda 6283$  DIB towards SN2008D in NGC2770 is slightly stronger ( $\text{EW } \lambda 6283/\text{E(B-V)} = 1200 \text{ m}\text{\AA}$ ) than the Galactic average ( $\text{EW } \lambda 6283/\text{E(B-V)} = 900 \text{ m}\text{\AA}$  Luna et al. (2008)), while the  $\lambda 5780$  DIB is a little weaker ( $\text{EW } \lambda 5780/\text{E(B-V)} \sim 350 \text{ m}\text{\AA}$ ) than the Galactic average ( $\text{EW}(\lambda 5780)/\text{E(B-V)} = 460 \text{ m}\text{\AA}$ ). For single clouds the  $\lambda 5780$  and  $\lambda 6283$  DIB strengths show a reasonable correlation though variations in their ratios are common. Together with a slightly above average  $\lambda 5797/\lambda 5780$  ratio and the presence of multiple cloud components in the atomic lines this indicates that with SN2008D we probe an ensemble of diffuse clouds with varying local conditions.

For example, SN2006X probes a compact dense inter-

stellar cloud with  $\text{E(B-V)} \sim 1 \text{ mag}$  and shows a relative weak  $\lambda 6283$  DIB of  $177 \text{ m}\text{\AA}$  (compared to the Galactic average of  $900 \text{ m}\text{\AA}$  per  $\text{E(B-V)}$ ) (Cox & Patat 2008; Luna et al. 2008). The line-of-sight toward SN2008D instead probes at least two diffuse components and shows a relative strong  $\lambda 6283$  DIB ( $\text{EW} = 850 \text{ m}\text{\AA}$  or  $\text{EW}/\text{E(B-V)} = 1200 \text{ m}\text{\AA}$ ) even slightly stronger than the Galactic “average” relation  $\text{EW}(\lambda 5780)/\text{E(B-V)} \sim 350 \text{ m}\text{\AA}$  for SN2008D, and  $460 \text{ m}\text{\AA}$  for MW, and  $189 \text{ m}\text{\AA}$  ( $\text{EW}/\text{E(B-V)} = 630 \text{ m}\text{\AA}$ ) for SN2001el (Sollerman et al. 2005). The  $\lambda 5780$  DIB carrier is sensitive to UV radiation and becomes stronger when exposed to UV radiation. The  $\lambda 5780$  is relatively weak with respect to the Galactic average, while the 6283 is stronger. Although generally these two DIBs show some correlation ratios that clearly differ between different sightlines.

#### 4.3. Star formation rates and ages of the stellar population

The local as well as the global SFR in NGC 2770 was determined by using the  $\text{H}\alpha$  flux and the conversion by Kennicutt (1992). The SFRs at the four different slit positions are given in Table 3 as  $\text{SFR kpc}^{-2}$ . We did the same for a range of regions within NGC 2770 by using the image taken with the  $\text{H}\alpha$  filter with the continuum subtracted using the offband filter as described in Section 2. The SFR at the sites of SNe 2008D and 1999eh are com-

TABLE 3  
RESOLVED PROPERTIES OF NGC 2770

Position [arcsec]	12+log(O/H) (O3N2)	(N2)	E(B-V) [mag]	H $\alpha$ EW [Å]	SFR [ $10^{-3} M_{\odot}/\text{yr}/\text{kpc}^2$ ]
74.86	8.31	8.20	0.01	122.1	5.2
69.73	8.50	8.33	0.44	34.70	4.9
67.45 (08D)	8.38	8.30	—	—	2.7
61.37	—	8.40	—	25.04	2.1
57.38	8.66	8.25	0.89	34.32	5.1
53.77	8.44	8.37	2.22	35.75	5.3
51.11	8.23	8.32	4.20	35.09	4.9
40.28	8.53	8.65	3.12	14.21	3.1
37.81	8.49	8.40	2.00	28.19	6.7
31.35	—	8.58	—	17.55	3.6
0.0	8.71	8.45	3.74	38.85	38.2
-20.90	—	8.61	1.12	40.08	4.0
-31.92	8.67	8.40	1.90	83.27	14.7
-39.71	8.62	8.39	1.62	102.9	15.6
-48.83	8.59	8.38	0.82	122.1	18.2
-55.86	8.36	8.41	0.93	51.63	10.2
-51.37	8.38	8.28	1.72	52.52	5.8
64.60	8.28	8.22	0.82	229.8	15.8
59.66	8.32	8.23	1.64	50.07	4.9
57.38 (08D)	8.42	8.29	—	—	3.9
47.12	8.41	8.37	1.27	77.29	9.7
40.28	—	8.21	—	24.31	3.1
25.46	—	8.31	—	27.85	4.9
19.76	—	8.29	—	21.16	4.4
14.06	—	8.31	—	31.13	8.0
12.16	—	8.24	—	20.14	4.5
5.70	—	8.76	—	9.743	3.7
0.38	8.60	8.74	2.91	17.89	7.3
-1.90	—	8.40	2.88	32.19	12.0
-12.54	—	8.42	—	14.37	3.9
-19.76	—	8.73	—	15.95	2.8
-32.30	8.59	8.59	1.41	35.29	10.9
-34.77 (07uy)	—	8.53	—	—	8.1
-37.62	8.49	8.37	1.37	76.20	15.1
-51.68	—	8.52	2.23	221.6	3.6
-78.66	—	8.45	—	72.64	3.5
37.81 (08D)	—	8.33	—	—	10.7
22.04	8.52	8.40	1.41	30.53	10.2
3.23	—	8.49	2.25	22.36	9.8
-1.52	8.51	8.44	2.00	69.33	32.9
-26.79	—	8.51	—	71.93	11.1
-31.16 (99eh)	8.48	8.37	0.72	61.23	11.8
-35.34	8.35	8.37	2.04	74.66	11.2
34.50	8.40	8.39	0.59	119.9	2.8
30.00	8.49	8.48	1.12	44.25	1.2
27.25 (08D)	8.57	8.51	0.95	5.014	1.1
17.00	8.43	8.41	1.88	91.78	4.1
0.500	8.57	8.54	2.10	41.34	1.4
-10.50	8.58	8.56	2.34	38.31	1.1
-27.50	8.46	8.41	0.64	117.2	3.7
-40.00	8.43	8.50	0.87	19.61	0.3
-45.00	8.28	8.33	1.86	14.56	0.2

NOTE. — Measurements from the optical spectra, from top to bottom: slit through the major axis (slit1), slit through SN 2007uy and SN 2008D (slit2), slit through SN 2008D and SN 1999eh (slit3) and FORS spectra through SN 2008D (slit4). Metallicities and SFRs were calculated from the fluxes not corrected for the extinction. The error in the metallicities are around 0.2 dex.

parable but not especially high. SN 2007uy lies a few arcsec from two sites with higher SF. The local SFRs elsewhere in NGC 2770 vary from  $2 \times 10^{-3}$  to  $4 \times 10^{-1} M_{\odot} \text{ yr}^{-1} \text{ kpc}^{-2}$ . The total SFR from the H $\alpha$  image taking an elliptic aperture to include the entire galaxy yields a flux of  $6.1 \times 10^{-12} \text{ erg cm}^{-2} \text{ s}^{-1}$  or a SFR of  $0.42 M_{\odot} \text{ yr}^{-1}$  which is consistent with other measurements from the UV, IR and radio fluxes.

The H $\alpha$  EW is further correlated with the age of the underlying population at least in the first  $10^6$  to  $10^7 \text{ yr}$

TABLE 4  
EWS AND COLUMN DENSITIES FROM THE UVES SPECTRA

line id	$\lambda_{\text{rest}}$ [Å]	$\lambda_{\text{obs}}$ [Å]	EW [Å]	b [km s $^{-1}$ ]	log N [cm $^{-2}$ ]
Ca II K	3933.66	3961.00	$0.55 \pm 0.03$	$14.1 \pm 7.1$	$12.92 \pm 0.07$
		3961.20		$18.3 \pm 2.4$	$12.78 \pm 0.07$
Ca II H	3968.47	3996.05	$0.42 \pm 0.03$	$14.1 \pm 7.1$	$12.92 \pm 0.07$
		3996.25		$18.3 \pm 2.4$	$12.78 \pm 0.07$
Na I D2	5889.95	5930.92	$0.33 \pm 0.02$	$7.3 \pm 0.3$	$12.96 \pm 0.05$
		5931.21	$0.38 \pm 0.02$	$8.1 \pm 0.3$	$12.71 \pm 0.02$
Na I D1	5895.92	5936.94	$0.26 \pm 0.02$	$7.3 \pm 0.3$	$12.96 \pm 0.05$
		5937.23	$0.36 \pm 0.02$	$8.1 \pm 0.3$	$12.71 \pm 0.02$
DIB	5780.37	5821.5	$0.245 \pm 0.04$	—	—
DIB	5796.99	5837.4	$0.850 \pm 0.05$	—	—
DIB	6283.85	6328.0	$0.090 \pm 0.02$	—	—

NOTE. — Equivalent width measurements, b parameters and column densities (where applicable) of interstellar absorption lines in NGC 2770 along the line of sight to SN 2008D, all wavelengths are in air. EWs are given for both components in the Ca II and Na I absorption systems. Galactic rest DIB wavelengths are from Galazutdinov et al. (2000)

(see e.g. Zackrisson et al. 2001). Table 3 also lists the H $\alpha$  EW at the different parts within the four slits. We cannot determine the EW at the sites of SN 2008D and SN 2007uy as the continuum is strongly affected by the presence of the SNe and we can only measure the EW of the nearby sites. We find that the stellar populations close to the SN sites are not among the youngest ones. This is a bit surprising since the progenitors of SNe Ib are expected to be stars with masses  $> 30\text{--}40 M_{\odot}$  whose lifetimes are  $< 6\text{--}7 \text{ Myr}$  corresponding to a H $\alpha$  EW of  $> 100 \text{ Å}$  (see e.g. Sollerman et al. 2005). There seems to be a strong gradient (see Fig. 3) in NGC 2770 towards high EWs in the outskirts of the galaxy whereas the center has rather low EWs corresponding to an older population. However, the EWs near all three SN sites are not particularly high which does not suggest particularly young populations.

#### 4.4. Kinematics

The UVES high resolution data allow us to study the kinematics in the sightline towards SN 2008D. We use the FITLYMAN program in MIDAS (Fontana & Ballester 1995) to fit different components to the Na I D1 and D2 as well as the Ca II H & K lines and to determine column densities (see Table 4). The absorption lines are best fitted with two components which are at velocities of  $-9.21$  and  $10.01 \text{ km s}^{-1}$  for the Na I lines and  $-8.60$  and  $6.54 \text{ km s}^{-1}$  for the Ca II lines. As  $v=0 \text{ km s}^{-1}$ , we take the redshift of the center of the galaxy for which we adopt  $z = 0.007$  as determined from the ALFOSC spectra probing the center of the galaxy. The two components are very narrow and have Doppler b parameters of  $7.3$  and  $8.1 \text{ km s}^{-1}$  for Na I D and  $14.1$  and  $18.3 \text{ km s}^{-1}$  for Ca II, the turbulent b parameter is very small and was fixed to  $1 \text{ km s}^{-1}$ .

We compare the position of the absorption with the emission lines which are likely to originate in the SF regions where the SN reside. The emission lines have a width of around  $30 \text{ km s}^{-1}$  which is most likely due to the turbulence in the SF region. There is no velocity shift between the hydrogen and oxygen emission lines suggesting a common origin for both elements. The red-der component of all absorption lines is coincident with



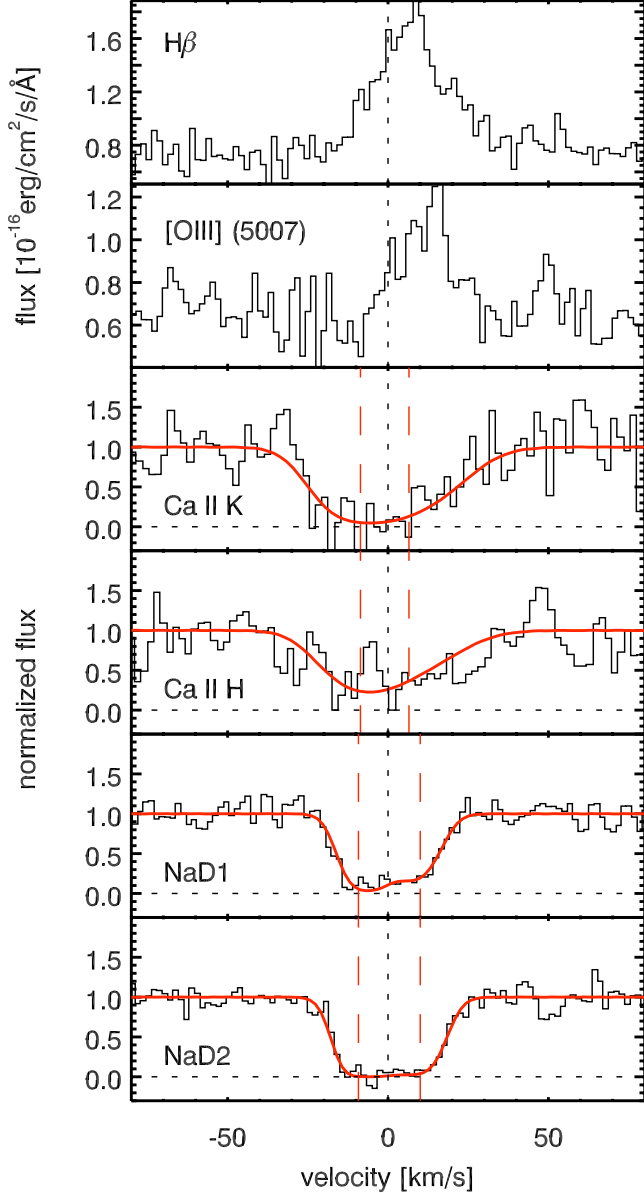


FIG. 5.— Fits to the Calcium and Sodium absorption lines in the UVES spectra and comparison to  $H\beta$  and  $[O\ III]$  emission lines. The dashed horizontal lines indicate the continuum level. Zero velocity corresponds to the center of the galaxy.

the position of the emission lines while the blue component is slightly shifted. This indicates that the absorbing material is most likely in front of the H II region of the SN. The position of the  $\lambda\ 5797$  and  $\lambda\ 6283$  DIBs are coincident with the other absorption lines whereas the  $\lambda\ 5780$  DIB is offset by about 40 km/s. A fit with fixing the center of the line to  $v = 0$  km/s gives almost the same  $\chi^2$  and a slightly lower line strength of 230 mÅ. There is also an intrinsic scatter of the rest wavelength of DIBs from different surveys which vary by 10–20 km/s. Due to the low line strengths and their intrinsically broad profile, it is not possible to distinguish different velocity components in the DIBs.

##### 5. NGC 2770 IN THE CONTEXT OF OTHER GRB AND SN HOSTS

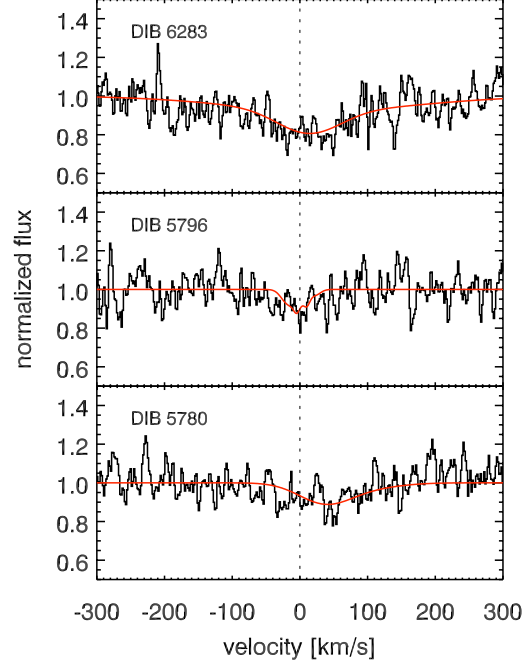


FIG. 6.— Fits to the DIBs detected in the UVES spectra of SN 2008D. Zero velocity corresponds to the center of the galaxy.

##### 5.1. Other galaxies with high SN rate

A number of galaxies exist that have had more than one SN detected in the optical. The record until today is for NGC 6946 with 9 SNe detected, and where all that could be classified were SNe II. NGC 6236 (M 83) had 6 SNe and there are 3 galaxies with 5 SNe (NGC 4303 (M61), NGC 4321 (M100) and NGC 2276 (Arp 25)). Furthermore, there are 9 galaxies with 4 SNe detected and 26 with 3 SNe of which one is NGC 2770 (complete up to May 30, 2008). We compiled this information from the CfA database including only galaxies with a catalogue name. We also include in our sample of frequent SN galaxies 4 galaxies that had 2 stripped-envelope SNe (to date NGC 2770 is the only one with 3). This sample is clearly biased but may still be useful for the comparison between frequent SN galaxies.

In Table 7 we list the SFRs, SNRs and specific SFRs weighted by the mass represented by the K-band luminosity for this sample. The radio SFRs are derived from Yun & Carilli (2002, eq. 15), the UV SFRs from Kennicutt (1992). For most galaxies, there is a good agreement between the UV and radio SFR except for NGC 2276 and NGC 3670. Usually, radio SFRs are higher than UV SFRs as the UV is affected by extinction in the host galaxy, which plays a larger role in edge on galaxies. In our sample, we do not account for the extinction correction and this was not done either for the GRB sample we use for comparison in Section 5.2. The SNRs were calculated from the nonthermal radio flux according to Condon (1992, eq. 18) which are based on the assumption that the radio flux comes from synchrotron radiation from electrons accelerated in the SN remnants.

It may appear surprising that the galaxies with the highest number of observed SNe do not necessarily have the highest (expected) SNRs as derived from radio data. However, most galaxies with 4 or more SN detected have an expected SNR between 1–4 in 10 yrs. This is con-

sistent with the number of actually detected SNe considering the small numbers and that SN observations in most of these galaxies have only been possible for the last few tens of years. NGC 2770 has a SSFR and SNR among the lowest in our sample and does not reflect the detected SN rate which could, however, be a statistical fluctuation (see Section 5.3).

An important bias in SN detections is the inclination of the galaxy observed as noted by several authors (e.g. Cappellaro et al. 1999). In our sample, the average number of SNe detected per galaxy drops towards higher inclinations, however, the distribution peaks around 30 deg inclination, most likely due to the low number of systems with lower inclinations. All of the galaxies with 5 and more SNe detected are seen nearly face-on. If we would have seen them edge-on, parts of the SNe might have been missed due to dust extinction or superposition with the bright central regions. Both issues are currently being addressed with SN searches in the IR (e.g. Mattila et al. 2007; Maiolino et al. 2002; Mannucci et al. 2003) and continuous monitoring of galaxies to perform image subtraction or observations in the radio (e.g. Cram et al. 1998).

It is interesting to note that many of the galaxies with frequent SN Ib/c occurrence are classified as starbursts, irregular or interacting with a neighboring galaxy whereas the galaxies with mainly SNe II or Ia are more “ordinary” spirals. This result is not surprising as SN Ib/c progenitors are likely more massive than those of SNe II and should therefore come from a younger population. Interaction between galaxies is considered as a possible trigger for star formation. In Fig. 8, we display the fraction of each SN type which occurred in the same type of galaxy. For the galaxy classification we adopted the values from de Vaucouleurs et al. (1991) which attributes values from  $-6$  to  $11$  with  $-6$  to  $0$  for elliptical galaxies,  $1-9$  spirals of increasing Hubble type and  $10$ ,  $11$  for irregular galaxies. SNe Ib/c seem to be more frequently detected in later type spirals compared to SN Type II, whereas SN Ia are rather evenly distributed over all galaxy types. van den Bergh et al. (2005) investigated the complete sample of SNe detected with the LOSS SN search and their hosts up to 2005 and do not find a significant difference between the Hubble Type of SN Type Ib/c and SN Type II. For our sample, we do only consider frequent SN hosts which introduces some bias in the sample. Panel I in Fig. 8, however, shows that, at least in our sample, there is a tendency of a higher fraction of SNe Ib/c over SNe II for spirals of later Hubble type.

Furthermore, some galaxies seem to produce only a certain type of SNe. In order to investigate this notion, we calculated the fraction of galaxies that only had one SN type detected from our sample of 44 frequent SN galaxies. 29 of those had SNe II out of which 51% had only SNe II, 13 had SNe Ib/c with 46% only having SNe Ib/c and 17 with SNe Ia of which only 29% had uniquely SNe Ia. In these numbers, we only include the classified SNe. It seems that indeed, galaxies with SNe II and Ib/c often only have one type of SN whereas this is less pronounced for SNe Ia. This result suggests that the SF history in those galaxies is rather uniform in the sense that SF has a common onset in time and first produces mainly SNe Ib/c expected to come from the most massive stars, whereas later on, when the dominant population

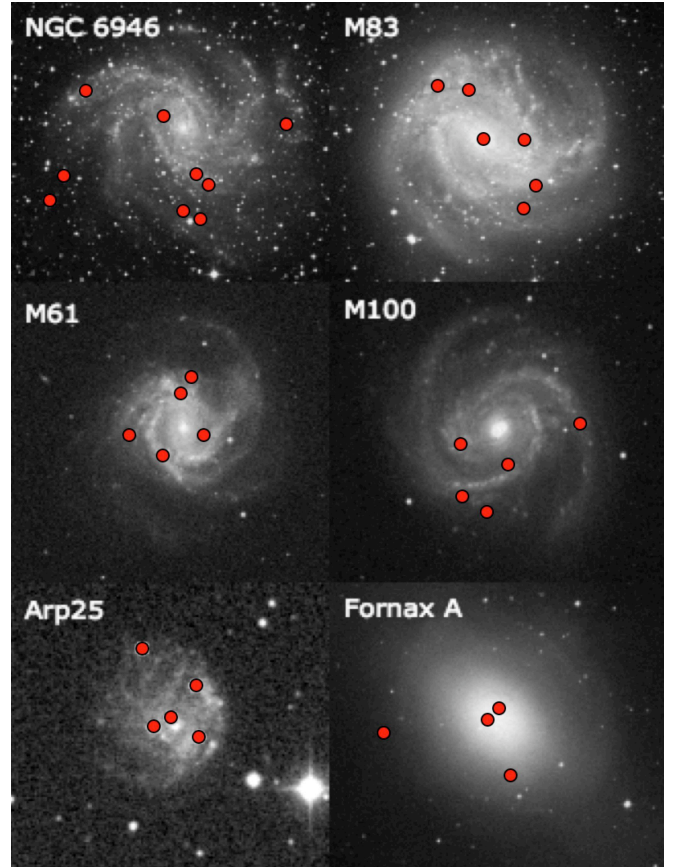


FIG. 7.— Images of the top 5 SN galaxies and Fornax A (only Ia SNe) with the positions of the SNe indicated.

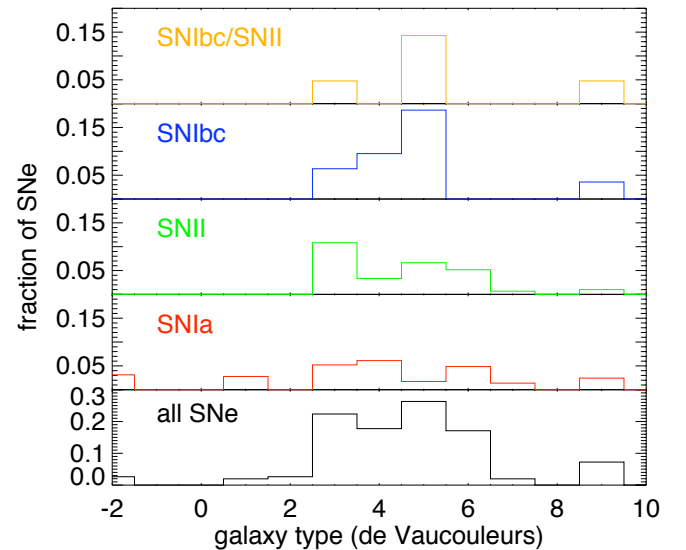


FIG. 8.— Fraction of detected SNe sorted according to the de Vaucouleurs classification (de Vaucouleurs et al. 1991) of their host galaxies. SNe Ib/c seem to be more concentrated towards later type spirals whereas SNe II seem to prefer earlier type spirals which are also expected to have an older stellar population. In general, most SNe are detected in spiral galaxies.

has become older, mainly SNe II are produced.

## 5.2. Comparison to other GRB and SN hosts

We now compare our sample of frequent SN galaxies to the hosts of long GRBs that are known to be connected

TABLE 5  
GALAXIES WITH FREQUENT SN OCCURRENCE

galaxy	incl. [deg]	SNe	SN types	gal. type	SFR (rad.) [M <sub>⊙</sub> yr <sup>-1</sup> ]	SFR (UV) [M <sub>⊙</sub> yr <sup>-1</sup> ]	SNR [yr <sup>-1</sup> ]	M <sub>stellar</sub> [M <sub>⊙</sub> ]	SSFR [Gyr <sup>-1</sup> ]
MW	...	4	...	SBc	1	1	0.0100	5 10 <sup>10</sup>	0.02
NGC 6946	29	9	II (6)	.SXT6.. <sup>d</sup>	3.125	3.143	0.0744	2.725×10 <sup>10</sup>	0.115
NGC 5236 (M83)	21	6	Ia (1)	.SXS5.. <sup>d</sup>	7.002	0.278	0.1666	6.506×10 <sup>10</sup>	0.108
NGC 4303 (M61)	25	5	II (4)	.SXT4..	11.17	10.09	0.2650	7.828×10 <sup>10</sup>	0.143
NGC 4321 (M100)	36	5	Ia (4), II (1)	.SXS4..	6.655	4.569	0.1579	9.942×10 <sup>10</sup>	0.067
NGC 2276 (Arp25)	21	5	II (2)	.SXT5.. <sup>d</sup>	17.55	...	0.4157	2.374×10 <sup>10</sup>	0.739
NGC 1316 (FornaxA)	56	4	Ia (3)	PLXS0P <sup>a</sup>	...	1.764	...	3.146×10 <sup>10</sup>	15.93
NGC 4038	65	4	Ia (1), Ib/c (1)	.SBS9P.. <sup>b,d</sup>	16.00	...	0.3867	...	...
NGC 3367	13	4	Ia, Ib/c, II	.SBT5.. <sup>a</sup>	11.30	...	0.2671	5.092×10 <sup>10</sup>	0.222
NGC 6754	60	4	II (1), Ia (1)	.SBT3..	2.551	...	0.0580	5.317×10 <sup>11</sup>	0.048
NGC 5468	24	4	II (1), Ia (2)	.SXT6..	...	...	...	...	...
NGC 4725	49	4	uncl.	.SXR2P.	0.393	1.475	0.0093	8.632×10 <sup>11</sup>	0.005
NGC 3184	15	4	uncl.	.SXT6..	0.275	...	0.0065	7.864×10 <sup>11</sup>	0.035
NGC 2841	65	4	Ia-p (2)	.SAR3*.. <sup>a</sup>	<0.343	0.287	<0.0082	2.668×10 <sup>11</sup>	0.013
NGC 3690	40	4	Ib (2), II (2)	.IB9P.. <sup>b,e</sup>	67.10	0.679	1.5873	7.283×10 <sup>11</sup>	0.921
NGC 521	...	3	II(1)	.SBR4..	0.819	...	0.0193	1.630×10 <sup>11</sup>	0.006
NGC 664	...	3	II(3)	.S..3*.	3.777	...	0.0888	3.938×10 <sup>10</sup>	0.096
NGC 735	...	3	II(1),Ic(1)	.S..3	0.830	...	0.0196	3.044×10 <sup>11</sup>	0.027
NGC 1058	21	3	Ib/c(1), II(1)	.SAT5..	0.019	...	0.0004	1.142×10 <sup>9</sup>	0.017
NGC 1084	56	3	II(2)	.SAS5..	8.110	...	0.1925	2.324×10 <sup>10</sup>	0.349
NGC 1097	47	3	II(3)	.SBS3.. <sup>f</sup>	7.180	0.172	0.1707	8.872×10 <sup>10</sup>	0.081
NGC 1365	58	3	II(2)	.SBS3..	15.23	...	0.3619	1.316×10 <sup>11</sup>	0.116
NGC 1448	79	3	Ia(1), II(2)	.SA.6*/	1.394	...	0.0331	2.051×10 <sup>10</sup>	0.068
NGC 1559	56	3	II(2), Ia(1)	.SBS6..	8.049	...	0.1912	1.841×10 <sup>10</sup>	0.437
UGC 1993	...	3	Ia, II	.S..3..	...	...	...	...	...
NGC 2207	54	3	Ib(1), Ib/c(1)	.SXT4P.. <sup>b</sup>	29.69	...	0.7035	6.953×10 <sup>10</sup>	0.427
NGC 2770	72	3	Ib(3)	.SAS5*.	0.586	0.638	0.0139	9.821×10 <sup>9</sup>	0.059
NGC 3147	31	3	Ia, Ib	.SAT4.. <sup>f</sup>	7.393	...	0.1750	1.512×10 <sup>11</sup>	0.049
NGC 3627 (M66)	67	3	Ia, II(2)	.SXS3.. <sup>a,f</sup>	2.441	1.111	0.0581	4.086×10 <sup>10</sup>	0.060
NGC 3631	28	3	II (1)	.SAS5..	1.148	...	0.0276	1.492×10 <sup>10</sup>	0.077
NGC 3938	14	3	Ic,II	.SAS5..	0.426	0.816	0.0101	8.586×10 <sup>9</sup>	0.050
NGC 3947	31	3	Ia(1), II(1)	RSBT3..	2.070	...	0.0486	5.592×10 <sup>10</sup>	0.037
NGC 4157	90	3	II, uncl.(2)	.SXS3\$/\$	1.162	...	0.0276	1.184×10 <sup>10</sup>	0.098
NGC 4254 (M99)	...	3	II(1)	.SAS5..	25.09	12.29	0.5944	1.715×10 <sup>10</sup>	0.146
NGC 4374 (M84)	...	3	Ia(2)	.E.1... <sup>a,c,f</sup>	...	0.064	...	6.344×10 <sup>10</sup>	1.104
NGC 4527	71	3	Ia(1)	.SXS4.. <sup>a</sup>	5.817	...	0.1380	8.834×10 <sup>10</sup>	0.066
NGC 4939	...	3	II(1)	.SAS4.. <sup>f</sup>	4.971	...	0.1177	7.156×10 <sup>10</sup>	0.069
NGC 5033	70	3	II(2)	.SAS5.. <sup>f</sup>	2.775	0.393	0.0660	2.201×10 <sup>10</sup>	0.126
NGC 5253	90	3	I(1)	.I..9P* <sup>d</sup>	0.148	0.079	0.0035	1.445×10 <sup>9</sup>	0.102
NGC 5457 (M101)	7	3	II(1)	.SXT6..	0.443	0.270	0.0105	6.307×10 <sup>9</sup>	0.070
NGC 5668	22	3	Ia, II	.SAS7..	0.603	...	0.0143	9.036×10 <sup>8</sup>	0.668
NGC 3810	...	2	Ib(1), Ic (1)	.SAT5..	1.249	...	0.0297	1.134×10 <sup>10</sup>	0.110
NGC 7714	42	2	Ib/c(2)	.SBS3*P <sup>a,d,e</sup>	1.258	0.952	0.0298	1.704×10 <sup>10</sup>	0.074
NGC 4568	65	2	Ib(1), Ic (1)	(SAbc) <sup>b</sup>	6.391	1.128	0.1514	8.751×10 <sup>10</sup>	0.073
NGC 3464	50	2	Ib(1), Ic(1)	.SBT5..	...	...	...	...	...

NOTE. — Complete sample of all galaxies with  $\geq 3$  SNe and 5 galaxies with 2 stripped envelope SNe, compiled from the CfA SN database. The classifications are adopted from RC3<sup>§</sup>, for those galaxies without RC3 classifications, we use the classification from NED. The adopted T value is the number in the classification code for spirals, the only elliptical galaxy, NGC 1316 has T=-2. Radio data, UV flux and K-band luminosity are taken from NED where available. SNRs are derived from radio data according to Condon (1992, eq. 18), SFRs are from Yun & Carilli (2002, eq. 15) for radio and Kennicutt (1992) for UV SFRs.

<sup>a</sup>low ionization nuclear emission line region (LINER)

<sup>b</sup>interacting galaxy

<sup>c</sup>low excitation radio galaxy (LERG)

<sup>d</sup>starburst

<sup>e</sup>Wolf-Rayet galaxy

<sup>f</sup>Seyfert galaxy

<sup>§</sup>1st column: R = outer ring; P = pseudo outer ring; C = compact; D = dwarf, 2nd column: E, S, I, P: elliptical, spiral, irregular, peculiar, 3rd column: X = transition between A (no bar) and B (barred galaxy). "++": transition between elliptical and lenticular galaxies (E/S0); 4th column: T = transition between s (no inner ring) and r (strong inner ring), number = ellipticity for an elliptical galaxy: 0 = round, 6, 7 = edge-on; 0 = I0 galaxies; 5th column: lenticulars: -, 0, or + (lenticular stages), spirals: Hubble stage: 0 for 0/a, 1 for a, ... 9 for m, for Magellanic irregulars, always 9; 6th column: Uncertainty (\* or ), P (minor peculiarity), or / = sp (spindle; an edgewise galaxy); 7th column: same as 6th, if needed.

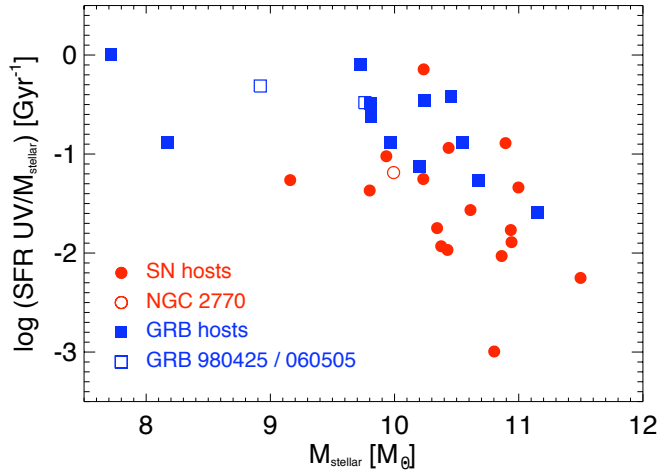


FIG. 9.— Specific SFR from the UV versus stellar mass derived from the  $K$ -band luminosity for GRB hosts (blue squares) and the sample of frequent SN galaxies (red dots) presented in Tab. ???. The GRB hosts specifically mentioned in Sec. ?? and NGC 2770 are plotted as empty symbols.

to broadlined SNe Ic. For the GRB hosts, we take the sample from Castro Cerón et al. (2008) which lists the UV SFRs derived from the relations of Kennicutt (1992) as well as the stellar masses derived from the restframe  $K$  band luminosity. GRB hosts have generally lower masses ( $\log M_{\text{stellar,SN}} = 10.71 M_{\odot}$ ,  $\log M_{\text{stellar,GRB}} = 10.36 M_{\odot}$ ) and higher SFRs ( $\text{SFR}_{\text{GRB}} = 2.9 M_{\odot} \text{ yr}^{-1}$ ,  $\text{SFR}_{\text{SN}} = 2.0 M_{\odot} \text{ yr}^{-1}$ ) than the frequent SN hosts from our sample. This leads to a higher SSFR for GRB hosts (0.075 and 0.32  $\text{Gyr}^{-1}$  for SN and GRB hosts respectively) even though the two samples overlap partially. We note that the masses derived in Castro Cerón et al. (2008) are about two times higher than the masses in the sample Savaglio et al. (2008) which partially overlap with the sample of Castro Cerón et al. (2008). This difference is partly explained by the use of different assumptions for the ratio  $M_{\text{stellar}}/L_K$  in both works. NGC 2770 has a SSFR close to the average in the frequent SN host sample, but a somewhat lower mass, but the SSFR lies clearly in the lower end of the distribution of long GRB hosts.

The hosts of broadlined SNe Ic from the sample of Modjaz et al. (2008a) have SFRs comparable to those of GRB hosts, but most likely smaller SSFRs due to their higher masses. As mentioned above, hosts of broadlined SNe Ic have higher metallicities than nearby GRB hosts which always have subsolar metallicities, some of them even down to 1/10 solar (for a complete sample see Savaglio et al. 2008, and references therein). Modjaz et al. (2008a) also note that the properties of the hosts of broadlined SNe Ic are consistent with those of normal nearby starforming spiral galaxies.

Some nearby GRB hosts are also different from the usual picture of low mass, high SF GRB hosts. The host of GRB 980425, connected to SN 1998bw (broadlined SN Ic) is a spiral galaxy with not particularly high SF in most parts of the galaxy, 1/3 of the global SF derived from this galaxy comes from a very luminous Wolf-Rayet (WR) region close to the GRB site (Christensen et al. 2008). The host of GRB 060505, a long GRB without SN, is a spiral galaxy and displays relatively high SF and a low metallicity at the site of the GRB (Thöne et al. 2008), but not in the galaxy in general, even though

the SF is still higher than in NGC 2770. It is still an open question whether GRB hosts are a special population of star-forming galaxies or following the general trend of other galaxies with redshift.

### 5.3. SN detection rates and the probability of finding 3 SNe in NGC 2770 in 10 years

NGC 2770 apparently has a high observed SN Ib rate with 3 explosions within ten years. Indeed, although 39 more galaxies are known to have had 3 or more SNe, no other galaxy has had more than two Ib/c SNe. Is this unexpected?

To date, no independent measurement of the SN rate of SNe Ib exists. In most cases (e.g. Dahlen et al. 2004; Cappellaro et al. 2005) rates in the literature are given for all Core Collapse Supernovae (CC SNe) together. Such results are, however, dominated by SNe II, which are the most frequent SNe. Some papers list at least SNe Ib/c and SNe II separately (e.g. Cappellaro et al. 1999; Mannucci et al. 2007).

The rate measurements are either volumetric in case of higher- $z$  SN surveys (e.g. Dahlen et al. 2004; Neill et al. 2006), or galaxy monitoring type searches, i.e. searches that look repetitively with a given cadence at a sample of galaxies. This kind of search usually has a number of biases, such as the frequency of observations, the limiting magnitudes achieved, the techniques used for detection or the galaxy inclination, and are restricted to lower or intermediate redshift (Cappellaro et al. 1999; Botticella et al. 2008).

Unlike SNe Ia, where an accurate and complete volumetric SN rate at low redshift has been measured (Dilday et al. 2008), the most recent results for CC-SNe is still from Cappellaro et al. (1999). Making estimates to correct for a number of biases, (Cappellaro et al. 1997) combine the results of 5 different supernova searches (including pre-CCD data) and obtain a rate of  $0.08 \pm 0.04 \times (H_0/75)^2 \text{ SNU}$  for SNe Ib/c (1 SNU = 1 SN per 100 yr per  $10^{10} L_{\odot}^B$ ). This rate increases to  $0.14 \pm 0.07 \times (H_0/75)^2$  if one only takes Sbc-Sd type galaxies. For NGC 2770, we find a B-band luminosity from NED of  $1.1 \times 10^{10} L_{\odot}^B$ . Assuming a Poissonian distribution for supernova events, the probability of NGC 2770 to have 3 SNe Ib/c in a decade is then  $6.1 \times 10^{-7}$ . The probability of getting 3 SN Ib events is even smaller.

We cross-check our expected number of SN events in NGC 2770 with Mannucci et al. (2007), who normalized the SN rate to the  $K$ -band luminosity (SNUK) by using the same sample of SN host galaxies as Cappellaro et al. (1999). The  $K$ -band luminosity is a better indicator of the stellar mass than the  $B$ -band luminosity which traces mostly the young star population. With a  $K$  band magnitude of 9.57 for NGC 2770 and by comparing with their predicted rates for Sbc galaxies (Mannucci et al. 2007, Tab. 2) we calculate a probability of  $1.5 \times 10^{-6}$  for NGC 2770 to have 3 SN Ib/c events within a decade. The two probabilities derived differ by a factor of about two. However, the chance probability for the observed SN rate at NGC 2770 is overall very small. In addition, the B-K color of NGC 2770 is 3.20, a value that does not indicate an extreme CC SN production (Mannucci et al. 2007). We note that the values derived here are only the probability to detect a SN from statistical considerations

and the luminosity of the galaxy and do not necessarily correlate with the expected SN rate from radio observations.

However, we also have to account for the number of observed galaxies to derive a number for the probability to find one such galaxy which produced 3 SNe Ib. SNe have been discovered in  $\sim 3500$  local galaxies but the total number of *monitored* galaxies is difficult to estimate, due also to the lack of information and uncertainties in individual amateur efforts. The results from Cappellaro et al. (1999) and Mannucci et al. (2007) are based on samples of 9346 and 8450 galaxies respectively. The LOSS search (Fillipenko et al. 2001), which is the most successful and systematic search in low- $z$ , monitors around 5000 local galaxies. If we now assume  $\sim 10000$  monitored galaxies, the chance of observing this high SN rate in any galaxy becomes  $0.6 - 1.5\%$  which is still a fairly low probability but given the uncertainties it could be consistent with a chance coincidence. This would also support the conclusions derived in Chapter 3 and Chapter 5.1 that NGC 2770 has no extraordinary global properties.

As a curiosity we add here that the same method of calculating probabilities, can to some extent explain the observed SN rates in the top SN producing galaxies (those with more than 5 observed SNe) with probabilities in the range  $10^{-3} - 10^{-1}$ , except the top SN producing galaxy, NGC 6946, which has a SED very similar to NGC 2770 (chance probability lower than  $10^{-4}$ ).

#### 6. NGC 2770B

We also obtained spectra of the neighboring galaxy, NGC 2770B, which has the same redshift as NGC 2770 (Fynbo et al. 2008) and can therefore be considered as a companion of NGC 2770. The galaxy consists of two “blobs” and we divide the 2D spectrum in 3 parts of which two are part of the first “blob” but show a small spatial separation in the emission lines in the 2D spectrum. Both regions shows very strong emission lines which points to a very young population undergoing heavy star formation. In Table 6 we list the emission lines detected as well as their fluxes.

We detect a large range of emission lines not detected in the spectra of NGC 2770 including [Ne III], H $\delta$ , Ca II, Na I, [O III]  $\lambda$  4363, He I, He II, [S III] and [Ar III] where the western “blob” of the galaxy shows most emission lines. [Ne III]  $\lambda$  3869 is exceptionally strong, especially in the western blob which indicates a large number of young stars. The spectrum resembles very much the nebular spectrum of young HII regions such as the Orion nebula in the MW. In this region, we also detect a clear Wolf-Rayet (WR) feature at 4640 Å (restframe). In Fig. 10, we show the spectrum of region one which has the strongest emission lines with an inset showing an enlargement of the WR feature.

The extinction as derived from the Balmer decrement using both H $\alpha$ /H $\beta$  as well as H $\beta$ /H $\gamma$  is consistent with zero. In order to determine the metallicity for NGC 2770B we cannot use any of the measurements which require [N II] that is only barely detected. This might be both an effect of the low metallicity and probably also a high temperature in the HII regions. Instead, we use the  $R_{23}$  parameter (Kewley & Dopita 2002) based on the line fluxes of H $\alpha$ , H $\beta$ , [O III] and [O II] which are all detected with high S/N in contrast to the spectra of NGC

TABLE 6  
LINE FLUXES IN NGC 2770B

Line	region 1 flux [ $10^{-15}$ erg cm $^{-2}$ s $^{-1}$ ]	region 2	region 3
[O II] $\lambda$ 3729	13.8	7.07	5.95
[Ne III] $\lambda$ 3869	15.5	2.43	1.71
H $\epsilon$	6.47	...	...
Ca II $\lambda$ 3969	9.69	0.73	1.06
H $\delta$	7.34	1.16	1.17
H $\gamma$	14.3	1.46	1.74
[O III] $\lambda$ 4363	3.23	...	0.28
He I $\lambda$ 4472	1.02	...	...
H $\beta$	29.6	4.37	4.04
EW[Å]	615	44.4	119
[O III] $\lambda$ 4960	71.1	8.88	7.81
[O III] $\lambda$ 5008	194	25.8	23.4
He I $\lambda$ 5876	3.11	0.13	0.49
[S III] $\lambda$ 6313	0.84	0.23	...
H $\alpha$	71.3	14.1	12.6
EW[Å]	2200	295	709
[N II] $\lambda$ 6585	0.51	0.04	0.14
[S II] $\lambda$ 6718	0.97	0.54	0.30
[S II] $\lambda$ 6732	2.60	0.19	0.89
Ne II $\lambda$ 7024	1.14	0.68	0.45
He II $\lambda$ 7065	0.63	...	...
[Ar II] $\lambda$ 7135	1.76	0.33	0.29
[O II] $\lambda$ 7330	1.81	...	...
12+log(O/H)	7.19	7.29	7.26
E(B-V)	0	0	0
SFR arcsec $^{-2}$	0.025	0.0049	0.0043

NOTE. — Fluxes and properties for three regions in NGC 2770B. The metallicity has been derived from the  $R_{23}$  parameter, the extinction from the Balmer line decrement, the SFR from H $\alpha$  and is listed as SFR/arcsec $^2$ .

2770. The metallicities we derive are among the lowest detected for nearby galaxies with 1/30 to 1/25 solar.

In two of the three spectra extracted from NGC 2770B, we also detected the [O III]  $\lambda$  4363 line which allows us to determine the electron temperature. From the electron temperature, it is possible to derive directly the abundances of O $^+$ /H and O $^{++}$ /H by using the method described by Izotov et al. (2006, eq. 1, 2, 4 and 5) and assuming that  $T_e(\text{O II}) = -0.577 + T_e(\text{O III})[2.065 - 0.498 T_e(\text{O III})]$  which Izotov et al. (2006) suggests for low metallicities (eq. 14). We then get values of  $T_e(\text{O II}) = 1.4 \times 10^4$  K for region 1 and  $T_e(\text{O II}) = 1.2 \times 10^4$  K for region 3 which gives metallicities of 12+log(O/H)=7.1 and 7.6 respectively. The value for region 1 agrees very well with the one derived from  $R_{23}$  whereas the value for region 3 from the  $T_e$  method is higher. We note, however, that the [O III]  $\lambda$  4363 line in region 3 was not detected with high significance.

The SFR in the eastern blob is comparable to the SFR in the nucleus of NGC 2770, however in the western part it is about an order of magnitude higher than in any region in NGC 2770. The very high EW of the H $\alpha$  line also indicate a dominant stellar population of only a few Myrs. We also calculate the global SFR from collapsing the entire spectrum of NGC 2770B and obtain a SFR of  $0.11 M_\odot \text{ yr}^{-1}$ . We obtained images from the 2MASS catalogue in  $K_s$  band and determined a magnitude of  $K_s = 15.3$  mag for NGC 2770B. Assuming a mass-to-light ratio of 0.4, the median value adopted by Castro Cerón et al. (2008) for GRB host galaxies, and taking eq. 1 from Castro Cerón et al. (2008), we determine a mass of only  $\log M_* = 7.65 M_\odot$ . Together with the SFR derived from



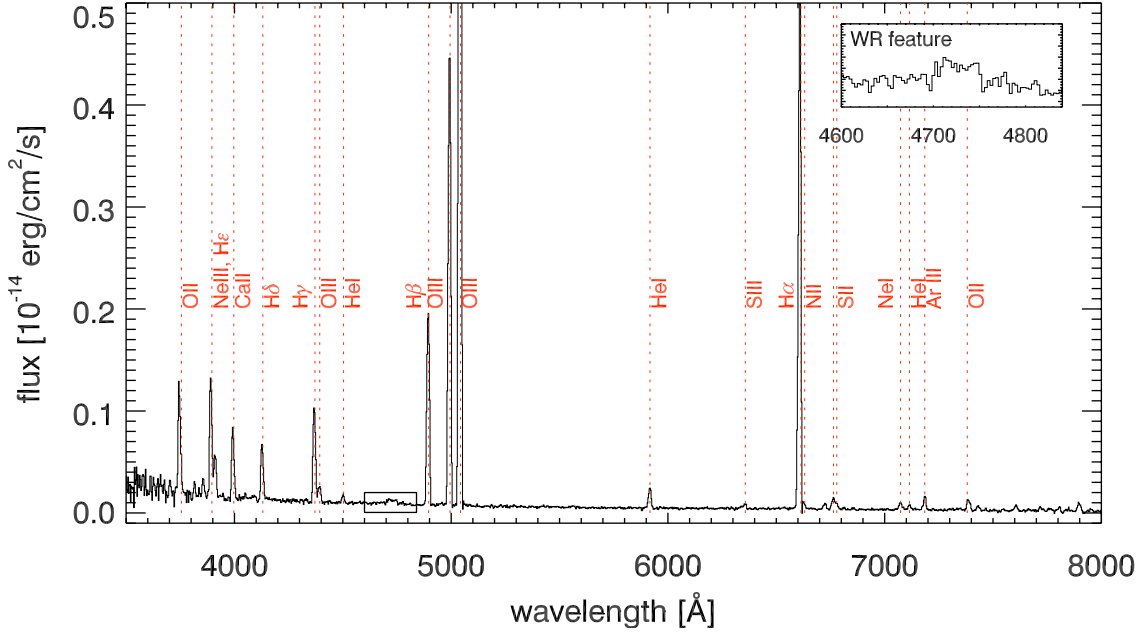


FIG. 10.— Spectrum of the region 1 in NGC 2770B which has the strongest emission lines. The emission lines of [O III] and H $\alpha$  have been cutted in order to enlarge the scale to show the weaker emission lines.

H $\alpha$ , this gives a very high specific SFR of  $0.39 \text{ Gyr}^{-1}$ .

NGC 2770B is a rather unusual galaxy compared to its massive neighbour NGC 2770. The fact that no SN has been detected (yet) in this galaxy is likely only due to its very low total mass so is the expected observed SN rate. It is also one of the most metal poor galaxies ever detected (see e.g. Izotov et al. 2006) which further indicates a very young stellar population. What triggered this high SFR in NGC 2770B remains unclear. It is also interesting that the most metal poor region has a clear detection of a WR feature. WR stars do only occur in a very narrow time window after the onset of a starburst between  $2$  and  $5 \times 10^6$  yr and are therefore a good tracer of the SF history. Models for WR stars predict a strong metallicity dependence on the wind which produces these features (e.g. Vink et al. 2001). However, there are a number of low metallicity galaxies with detected WR features which have challenged this model (e.g. Brinchmann et al. 2008). Possible explanations are that there are actually more WR stars produced than predicted from the models or that WR stars which are rapidly rotating can form at much lower metallicities. Rapidly rotating WR stars have also been suggested as progenitor for GRBs. Overall, NGC 2770B seems to be a exceptional galaxy that is potentially interesting for future studies.

## 7. CONCLUSIONS

We have investigated the properties of the three SN sites in NGC 2770, the host of three SNe Ib, and the other regions in the host along 4 longslit positions. Previous observations in all wavelengths from UV to radio allow us to fit the SED of NGC 2770 and derive a range of global properties from it. We then set NGC 2770 in context to a sample of galaxies with frequent SN occurrence (3 or more SNe detected) and also compute the probability to detect three SNe Ib in a galaxy within only 10 years as it was the case for NGC 2770. From this analyses, we then conclude the following:

- NGC 2770 has global properties similar to the MW, even though it has a higher number of SNe observed. Its SFR and SNR are around the average of other nearby spiral galaxies and our sample of frequent SN galaxies.
- The only outstanding property of NGC 2770 is its high HI mass which indicates a large reservoir for forming stars.
- The metallicities at the SN sites in NGC 2770 are around 0.5 solar which is similar to the values observed for nearby GRB sites, but lower than for broadline SN Ic sites.
- Almost half of the galaxies with SNe II and Ib/c only have one type of SN which is likely connected to the age of the dominant stellar population. Galaxies producing SNe Ib/cs have a higher deVaucouleurs number than those producing SN II.
- SN and GRB hosts seem to be somewhat different in terms of SFRs and masses.
- The probability to detect 3 SNe Ib in a galaxy is 0.6 to 1.5 % assuming 10,000 monitored galaxies.

It therefore seems to be likely that observing 3 SNe Ib in NGC 2770 was only a chance coincidence. NGC 2770 is by no means a special galaxy that would be predestined to produce only stripped-envelope SNe. In fact its properties are not typical for galaxies with (frequent) SN Ib/c occurrence. However, it might also imply that the local properties at the SN sites are more important, at least in some galaxies, to produce a certain type of SN than its global properties.

CT and PMV want to thank Cédric Ledoux for the reduction of the UVES spectra.

The Dark Cosmology Centre is funded by the Danish National Research Foundation. We thank the staff and the NOT and the VLT to perform the observations. In this work we made use of the NASA Extragalactic Database (NED). NED is operated by the Jet Propul-

sion Laboratory, California Institute of Technology, under contract with the National Aeronautics and Space Administration. JS is a Royal Swedish Academy of Sciences Research Fellow supported by a grant from the Knut and Alice Wallenberg Foundation.

## REFERENCES

- Asplund, M., Grevesse, N., Sauval, A. J., Allende Prieto, C. and Kiselman, D. 2004, *A&A* 417, 751
- van den Bergh, S., Li, W. & Filippenko, A. V. 2005, *PASP*, 117, 773
- Botticella, M. T. et al. 2008, *A&A*, 479, 49
- Brinchmann, J., Kunth, D., & Durret, F. 2008, *A&A*, 485, 657
- Broeils & Rhee 1997, *A&A*, 324, 877
- Cappellaro, E., Turatto, M., Tsvetkov, D. Y., Bartunov, O. S., Pollas, C., Evans, R. & Hamuy, M. 1997, *A&A*, 322, 431
- Cappellaro, E., Evans, R. & Turatto, M. 1999, *A&A*, 351, 459
- Cappellaro, E. et al. 2005, *A&A*, 430, 83
- Castro Cerón J.M., Michałowski M., Hjorth J., Watson D.J., Fynbo J.P.U., Gorosabel J., 2006, *ApJ*, 653, L85
- Castro Cerón J.M., Michałowski M.J., Hjorth J., Malesani D., Gorosabel J., Watson D., Fynbo J.P.U., 2008, *ApJ*, submitted, preprint: [arXiv:0803.2235v1](https://arxiv.org/abs/0803.2235v1) [*astro-ph*]
- Christensen, L., Hjorth, J., & Gorosabel, J. 2004, *A&A*, 425, 913
- Christensen, L., Vreeswijk, P., Sollerman, J., Thöne, C., Le Floc'h, E. & Wiersema, K. 2008, *A&A*, submitted
- Crowther, P. A., Dessart, L., Hillier, D. J., Abbott, J. B., & Fullerton, A. W. 2002, *A&A*, 392, 653
- Cobb, B. E., Baylin, C. D., van Dokkum, P. G., Buxton, M. M., & Bloom, J. S. 2004, *ApJ*, 608, L93
- Condon, J. J. 1992, *ARA&A*, 30, 575
- Condon J.J., Cotton W.D., Greisen E.W., Yin Q.F., Perley R.A., Taylor G.B., Broderick J.J., 1998, *AJ*, 115, 1693
- Cox, N. L. J., & Patat, F. 2008, *A&A*, 485, L9
- Cram, L., Hopkins, A., Mobasher, B., & Rowan-Robinson, M. 1998, *ApJ*, 507, 155
- Crockett, R. M. et al. 2007, *MNRAS*, 381, 835
- Crockett, R. M. et al. 2007, *ApJ*, 672, L99
- Crowther, P. A., Dessart, L., Hillier, D. J., Abbott, J. B., & Fullerton, A. W. 2002, *A&A*, 392, 653
- Cutri, R. M., et al. 2003, The IRSA 2MASS All-Sky Point Source Catalog, NASA/IPAC Infrared Science Archive. <http://irsa.ipac.caltech.edu/applications/Gator/>
- Dahlen, T. et al. 2004, *ApJ*, 613, 189
- Della Valle, M., et al. 2006, *Nature*, 444, 1050
- Dekker, H., et al. 2000, *Proc. SPIE*, 4008, 534
- Dilday, B. et al. 2008, [arXiv:0801.3297](https://arxiv.org/abs/0801.3297) [*astro-ph*]
- Dong & Robertis 2006, *ApJ*, 131, 1236
- Dressel L.L., Condon J.J., 1978, *ApJS*, 36, 53
- Filippenko, A. V., Li, W. D., Treffers, R. R. & Modjaz, M. 2001, proceedings of the IAU Colloq. 183: Small Telescope Astronomy on Global Scale, ed. Paczynski, B., Chen, W.-P., Lemme, C., ASP conf. series, vol. 246, 121
- Fontana, E., & Ballester, P. 1995, *ESO Messenger* 80, 37
- Foley, S., Watson, D., Gorosabel, J., Fynbo, J. P. U., Sollerman, J., McGlynn, S., McBreen, B., & Hjorth, J. 2006, *A&A*, 447, 891
- Fruchter, A. S. et al. 2006, *Nature*, 441, 463
- Fynbo, J. P. U. et al. 2006, *Nature*, 444, 1047
- Fynbo, J. P. U., Malesani, D., Augusteijn, T., & Niemi, S.-M. 2008, *GRB Coordinates Network*, 7186, 1
- Gal-Yam, A., et al. 2004, *ApJ*, 609, L59
- Gal-Yam, A. et al. 2006, *Nature*, 444, 1053
- Gal-Yam, A. et al. 2007, *ApJ*, 656, 372
- Galama, T. J. et al. 1998, *Nature*, 395, 670
- Gehrels, N. et al., 2004, *ApJ*, 611, 1005
- Gehrels, N., et al. 2006, *Nature*, 444, 1044
- Gilmozzi, R. et al. 1987, *Nature*, 328, 318
- Heger, A., Fryer, C. L., Woosley, S. E., Langer, N. & Hartmann, D. H. 2003, *ApJ*, 591, 288
- Hendry, M. A. et al. 2006, *MNRAS*, 369, 1303
- Hjorth, J., et al. 2003, *Nature*, 423, 847
- Ho, L. C., Filippenko, A. V., & Sargent, W. L. W. 1997, *ApJS*, 112, 315
- Izotov, Y. I., Papaderos, P., Guseva, N. G., Fricke, K. J., & Thuan, T. X. 2006, *A&A*, 454, 137
- Izotov, Y. I., Papaderos, P., Guseva, N. G., Fricke, K. J., & Thuan, T. X. 2006, *A&A*, 454, 137
- Kelly, P. L., Kirshner, R. P., & Pahre, M. 2007, *ArXiv e-prints*, 712, [arXiv:0712.0430](https://arxiv.org/abs/0712.0430)
- Kennicutt, R. C. Jr. 1992, *ApJS*, 79, 255
- Kewley, L. J., & Dopita, M. A. 2002, *ApJS*, 142, 35
- Li, W. et al. 2007, *ApJ*, 661, 1013
- Luna, R., Cox, N. L. J., Satorre, M. A., García Hernández, D. A., Suárez, O., & García Lario, P. 2008, *A&A*, 480, 133
- MacFadyen, A. I., & Woosley, S. E. 1999, *ApJ*, 524, 262
- Maiolino, R., Vanz, L., Mannucci, F., Cresci, G., Ghinassi, F., & Della Valle, M. 2002, *A&A*, 389, 84
- Malesani, D. et al. 2004, *ApJ*, 609, L5
- Mannucci, F., et al. 2003, *A&A*, 401, 519
- Mannucci, F., Della Valle, M., Panagia, N., Cappellaro, E., Cresci, G., Maiolino, R., Petrosian, A. & Turatto, M. 2005, *A&A*, 433, 807
- Malesani, D. et al. *ApJ*, submitted, preprint: [arXiv:0805.1188v1](https://arxiv.org/abs/0805.1188v1) [*astro-ph*]
- Martin C., et al., 2003, In: Blades J.C., Siegmund O.H.W. (eds.) *Future EUV/UV and Visible Space Astrophysics Missions and Instrumentation*. Edited by J. Chris Blades, Oswald H. W. Siegmund. Proceedings of the SPIE, Volume 4854, pp. 336-350 (2003)., vol. 4854 of Presented at the Society of Photo-Optical Instrumentation Engineers (SPIE) Conference, 336-350
- Martin D.C., et al., 2005, *ApJ*, 619, L1
- Matheson, T., et al. 2003, *ApJ*, 599, 394
- Mattila, S. et al. 2007, *ApJ*, 659, L9
- Maund, J. R. and Smartt, S. J. and Schweizer, F., *ApJ*, 630, L33
- Michałowski M.J., Hjorth J., Castro Cerón J.M., Watson D., 2008, *ApJ*, 672, 817
- Mirabal, N., Halpern, J. P., An, D., Thorstensen, J. R., & Terndrup, D. M. 2006, *ApJ*, 643, L99
- Modjaz, M., et al. 2006, *ApJ*, 645, L21
- Modjaz, M. et al. 2008a, *AJ*, 135, 1136
- Modjaz, M. et al. 2008b, *ApJ*, submitted, [arXiv:0805.2210](https://arxiv.org/abs/0805.2210) [*astro-ph*]
- Moshir M., et al., 1990, In: *IRAS Faint Source Catalogue*, version 2.0 (1990), 0
- Munari, U., & Zwitter, T. 1997, *A&A*, 318, 269
- Neill, J. D. et al. 2006, *AJ*, 132, 1126
- Ofek, E. O., et al. 2007, *ApJ*, 662, 1129
- Osterbrock, D. E. 1989, *Astrophysics of Gaseous Nebulae and Active Galactic Nuclei*, University Science Books, Mill Valley, CA
- Pettini, M., & Pagel, B. E. J. 2004, *MNRAS*, 348, L59
- Pian, E., et al. 2006, *Nature*, 442, 1011
- Rhee & Albada 1996, *A&ASS*, 115, 407
- Savaglio S., Glazebrook K., Le Borgne D., 2008, *ApJ*, submitted, [arXiv:0803.2718v1](https://arxiv.org/abs/0803.2718v1) [*astro-ph*]
- Schlegel, D. J., Finkbeiner, D. P., & Davis, M. 1998, *ApJS*, 80, 1
- Silva L., Granato G.L., Bressan A., Danese L., 1998, *ApJ*, 509, 103
- Smartt, S. J., Maund, J. R., Gilmore, G. F., Tout, C. A., Kilkenny, D., & Benetti, S. 2003, *MNRAS*, 343, 735
- Soderberg, A. M., et al. 2006, *Nature*, 442, 1014
- Soderberg, A. M., et al. 2008, *Nature*, 453, 469
- Sollerman, J., Cox, N., Mattila, S., Ehrenfreund, P., Kaper, L., Leibundgut, B., & Lundqvist, P. 2005, *A&A*, 429, 559
- Sollerman, J., Östlin, G., Fynbo, J. P. U., Hjorth, J., Fruchter, A., & Pedersen, K. 2005, *New Astronomy*, 11, 103
- Sollerman, J., et al. 2006, *A&A*, 454, 503
- Stanek, K. Z., et al. 2003, *ApJ*, 591, L17
- Staveley-Smith, xy & Davies, xy 1988, *MNRAS*, 231, 833
- Thomsen, B., et al. 2004, *A&A*, 419, L21
- Thöne, C. C. et al. 2008, *ApJ*, 677, 1151
- de Vaucouleurs, G. and de Vaucouleurs, A. and Corwin, Jr., H. G. and Buta, R. J. and Paturel, G. and Fouque, P., 1991, "Third reference catalogue of bright galaxies", vol. 1-3, XII, 2069, Springer Verlag Berlin, Heidelberg, New York

- Vink, J. S., de Koter, A., & Lamers, H. J. G. L. M. 2001, *A&A*, 369, 574
- Wainwright, C., Berger, E., & Penprase, B. E. 2007, *ApJ*, 657, 367
- Woosley, S. E., Heger, A., & Weaver, T. A. 2002, *Reviews of Modern Physics*, 74, 1015
- Woosley, S. E., & Heger, A. 2006, *ApJ*, 637, 914
- Xu, D., Zou, Y.-C., & Fan, Y.-Z. 2008, preprint: astro-ph/0801.4325
- Yun, M. S. & Carilli, C. L. 2002, *ApJ*, 568, 88
- Zackrisson, E., Bergvall, N., Olofsson, K. & Siebert, A. 2001, *A&A*, 375, 814
- Zeh, A., Klose, S., & Hartmann, D. H. 2004, *ApJ*, 609, 952